ELSEVIER

Research: Review

Selective membranes in water and wastewater treatment: Role of advanced materials

Kuichang Zuo [1,2], Kunpeng Wang [3], Ryan M. DuChanois [2,4], Qiyi Fang [2,5], Eva M. Deemer [2,6], Xiaochuan Huang [1,2], Ruikun Xin [1,2], Ibrahim A. Said [1,2], Ze He [2,7], Yuren Feng [1,2], W. Shane Walker [2,6], Jun Lou [2,5,*], Menachem Elimelech [2,4,*], Xia Huang [3,*], Qilin Li [1,2,5,7,*]

[1] Department of Civil and Environmental Engineering, Rice University, 6100 Main Street, Houston 77005, USA
[2] NSF Nanosystems Engineering Research Center for Nanotechnology-Enabled Water Treatment, Rice University, 6100 Main Street, Houston 77005, USA
[3] School of Environment, Tsinghua University, Beijing 100084, China
[4] Department of Chemical and Environmental Engineering, Yale University, New Haven, CT 06520-8286, USA
[5] Department of Materials Science and Nano Engineering, Rice University, 6100 Main Street, Houston, TX 77005, USA
[6] Department of Civil Engineering, The University of Texas at El Paso, El Paso, TX 79968-0513, USA
[7] Department of Chemical and Biomolecular Engineering, Rice University, 6100 Main Street, Houston, TX 77005, USA

Membrane separation has enjoyed tremendous advances in relevant material and engineering sciences, making it the fastest growing technology in water treatment. Although membranes as a broad-spectrum physical barrier have great advantages over conventional treatment processes in a myriad of applications, the need for higher selectivity and specificity in membrane separation is rising as we move to target contaminants at trace concentrations and to recover valuable chemicals from wastewater with low energy consumption. In this review, we discuss the drivers, fundamental science, and potential enabling materials for high selectivity membranes, as well as their applications in different water treatment processes. Membrane materials and processes that show promise to achieve high selectivity for water, ions, and small molecules—as well as the mechanisms involved—are highlighted. We further identify practical needs, knowledge gaps, and technological barriers in both material development and process design for high selectivity membrane processes. Finally, we discuss research priorities in the context of existing and future water supply paradigms.

Keywords: Selective membranes; Advanced materials; Water and wastewater treatment

Membranes in water and wastewater treatment

Clean water is a universal need for prosperity of human societies. Removing harmful chemicals from water and wastewater is necessary to protect public health and the environment. Due to their high efficiency, compact and modular design, and high level of automation, membrane separation processes are quickly replacing conventional treatment methods in water and wastewater systems. Their widespread implementation in water treatment and reuse as well as resource (e.g., nutrients and precious metals) recovery have undoubtedly benefited from the advances in membrane materials and relevant engineering sciences, which greatly improved treatment efficiency (e.g., water permeability) and reduced costs.

* Corresponding authors.
E-mail addresses: Zuo, K. (kz19@rice.edu), Lou, J. (jlou@rice.edu), Elimelech, M. (menachem.elimelech@yale.edu), Huang, X. (xhuang@tsinghua.edu.cn), Li, Q. (qilin.li@rice.edu).

 https://doi.org/10.1016/j.mattod.2021.06.013

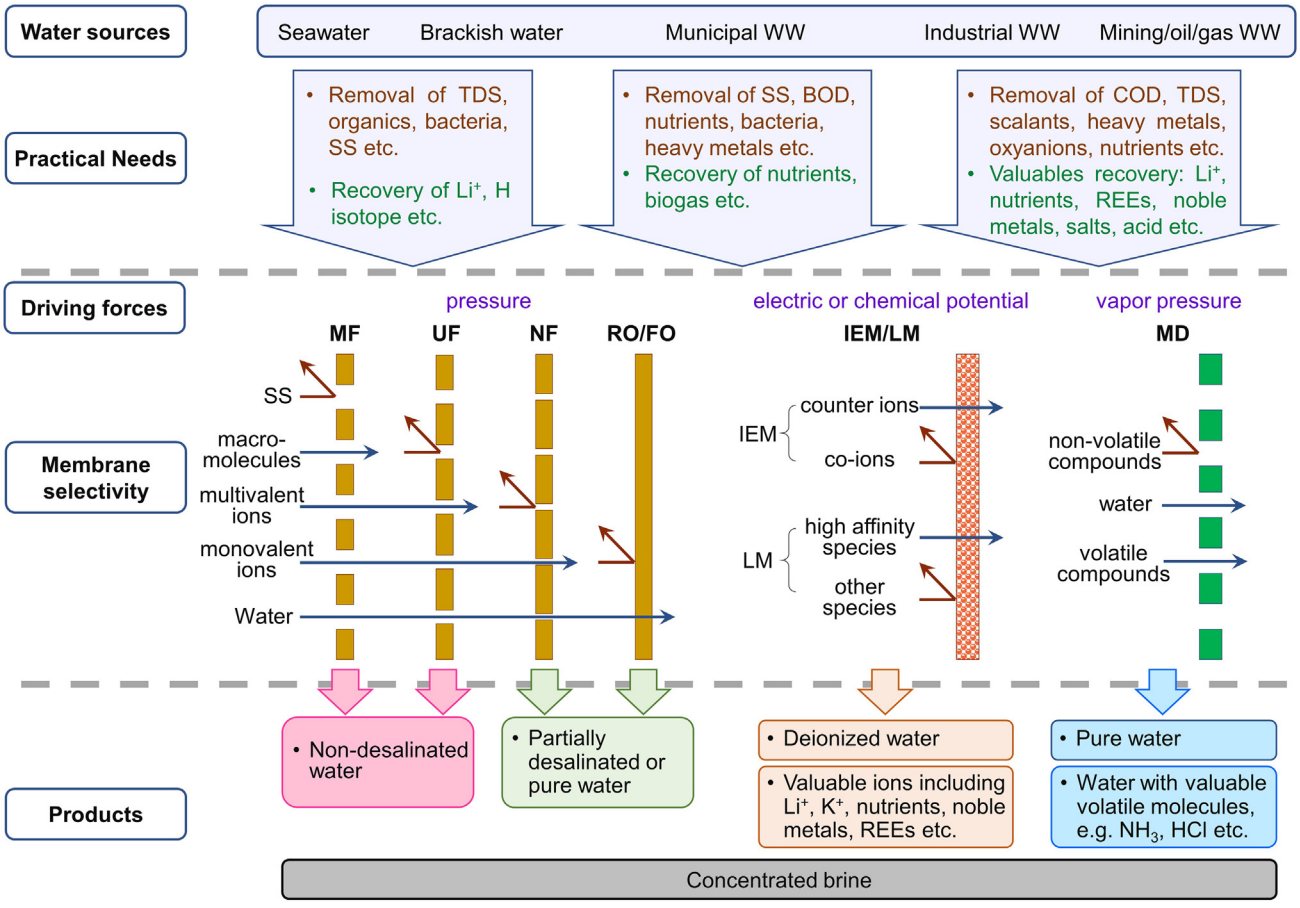

FIGURE 1

Water treatment membranes and their separation functions in water treatment. WW: wastewater; TDS: total dissolved solids; SS: suspended solids; BOD: biochemical oxygen demand; COD: chemical oxygen demand; REEs: rare earth elements.

Membranes can be categorized as either water-permeating membranes or solute-permeating membranes. Water-permeating membranes favour transport of water over the various solutes (e.g., salt ions and organic molecules), and have been widely used to remove unwanted contaminants in drinking water treatment, wastewater reclamation, and seawater desalination. They are used in many processes, including microfiltration (MF), ultrafiltration (UF), nanofiltration (NF), reverse osmosis (RO), forward osmosis (FO), and membrane distillation (MD). MF membranes are widely used in surface water treatment to remove suspended solids, including bacteria [1], and in membrane bioreactors in wastewater treatment to retain biomass and improve effluent quality [2,3]. UF is used extensively in the dairy [4,5] and pharmaceutical [6] industries to purify and concentrate chemicals of various molecular weights. In water treatment, it is increasingly used as pretreatment for NF and RO processes [7]. Both MF and UF remove contaminants by size exclusion, utilizing microscopic pores in the membrane. The market size of MF membranes is estimated to be USD 12.8 billion in 2022 [8], and that for UF will reach USD 5.5 billion by 2025 [9]. NF [10], RO [11], and FO [12] membranes reject a wide range of chemicals, including salt ions and other low molecular weight compounds by size exclusion and Donnan exclusion. They are utilized for softening, desalination, and wastewater reuse. The market size for RO and NF is projected to reach USD 13.5 billion [13] and 950 million [14] in 2025, respectively. Another type of membranes used for desalination are microporous hydrophobic MD membranes that separate chemicals based on their vapor pressure. MD membranes allow permeation of water vapor but retain liquid water and all dissolved species [15].

Solute permeating membranes including ion exchange membranes (IEMs) [16], and liquid membranes (LMs) [17–19] separate chemicals based on the affinity of the chemicals to the membrane. They allow high affinity solutes (e.g., salt ions and other charged or neutral solutes) to permeate, achieving water desalination and resource recovery. IEMs are often used in electrodialysis (ED) processes for water desalination, while LM is used in a liquid-liquid extraction process to immobilize the liquid extractant.

Drivers and needs for membrane selectivity

Despite the many advantages of membrane-based water treatment processes, increasing global water stress, more stringent regulations, and rising expenses for wastewater disposal demand higher water recovery, lower treatment cost, and greater value generation—all pointing to the need for high selectivity membranes.

An important driver for high selectivity membranes is the need to use alternative water sources with widely varying water qualities, e.g., brackish water, seawater, municipal and industrial wastewaters, and the diverging end-use of product waters. Although maximizing water recovery and minimizing brine volume while keeping the energy consumption low is the common goal, treatment needs can be vastly different, depending on the water source and end-use (Fig. 1). For example, in arid coastal areas where seawater is the main water source for potable and industrial uses, all pollutants and salt ions must be removed at very high levels. When reusing municipal wastewater, which has a much lower salt concentration than seawater, for direct or indirect potable applications, treatment must ensure very high rejection of wastewater contaminants, e.g., heavy metals, nutrients, organic contaminants including *N*-Nitrosodimethylamine (NDMA) and other disinfection by-products, perfluorinated alkyl substances, pharmaceutically active compounds, and personal care products; high salt rejection may be unnecessary and even undesirable. In this case, a selective membrane with high rejection of toxic and problematic contaminants but relatively low rejection for salt ions is needed.

Industrial wastewaters are highly diverse. Some may contain high concentrations of toxic compounds, but do not necessarily contain high salt concentrations. When reusing industrial wastewaters for non-potable applications, it may be unnecessary to remove the large number of chemicals in the wastewater that do not negatively impact the beneficial reuse. Ideally, membranes that selectively remove the problematic compounds would provide the most energy-efficient treatment. One of the main concerns in industrial wastewater is heavy metals (e.g., Pb^{2+}, As(III), Cr(VI)), which are regulated at parts-per-billion thresholds [20–22], driving the development of membranes with selectivity for heavy metals over common cations (e.g., Na^+, K^+, and Ca^{2+}) [23]. The need to remove toxic anions (e.g., F^-, Br^-)

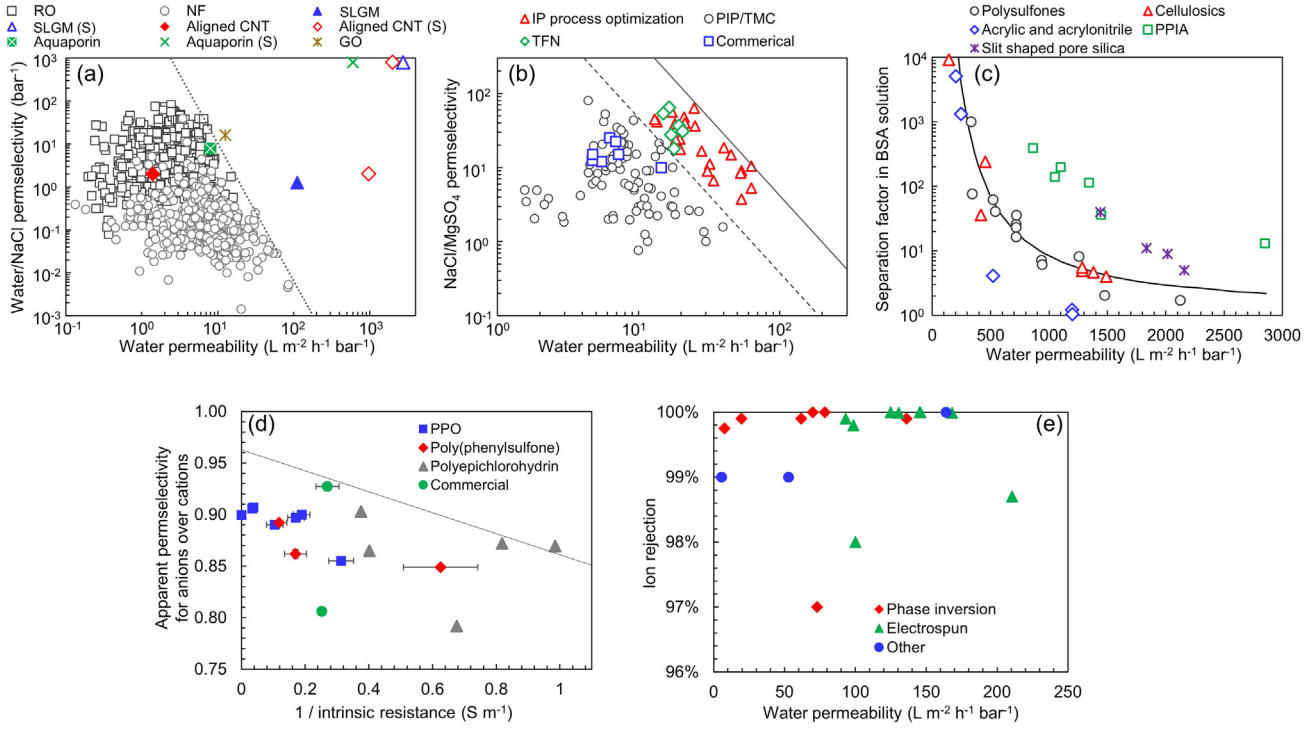

FIGURE 2

Trade-off between membrane selectivity and permeability and the role of advanced materials. (a) Water/NaCl separation by polyamide RO and NF membranes [33] and novel membrane materials. Solid triangle, asterisk, diamond, and cross or a cross in a solid square symbols represent single-layer graphene membrane (SLGM) [55], graphene oxide (GO) laminar membrane [56], vertically aligned CNT membrane [57] and aquaporin membrane [58] prepared in the laboratory, respectively, and the corresponding hollow shapes represent model-simulated separation performance of these materials [59–61]. The selectivity is defined as the ratio between water permeability coefficient over solute permeability coefficient [33], which is slightly different from Eq.1. Adapted from Ref. [33] and reproduced with permission of copyright © 2019 Elsevier B.V.; (b) Trade-off between water permeability and NaCl/$MgSO_4$ permeation selectivity of commercial and lab-prepared NF membranes [35]. Triangle and diamond symbols represent membranes prepared with optimized interfacial polymerization (IP) processes and advanced materials, respectively [28,62–73]. PIP/TMC, traditional polyamide NF membranes formed by IP using piperazine and trimesoyl chloride. TFN, thin film nanocomposite membranes. Adapted from Ref. [35] and reproduced with permission of copyright © 2018 American Chemical Society; (c) Trade-off between water permeability and bovine serum albumin (BSA) separation factor in traditional polysulfone, cellulosic, acrylic, and poly(*m*-phenylene isophthalamide) (PPIA) ultrafiltration membranes. The curve represents model calculations using a log–normal pore radius distribution [36]. The square and asterisk symbols represent novel membranes prepared with poly(m-phenylene isophthalamide) and porous silica, respectively [74,75]. Adapted from Ref. [36] and reproduced with permission of copyright © 2005 Elsevier B.V.; (d) Trade-off between permselectivity and membrane ionic resistance in anion exchange membranes prepared with various materials. PPO: Poly(2,6-dimethyl-1,4-phenylene oxide), reproduced with permission from Ref. [37]. Copyright © 2013 American Chemical Society; (e) Steady state salt rejection and water vapor permeability of MD membranes in desalination of saltwater [76–89].

and oxyanions (e.g., ClO_4^-, BrO_4^-, and NO_3^-) from industrial waste streams requires selectivity between target and background anions (e.g., Cl^-). In mining and oil and gas production, reusing wastewater requires removing sparsely soluble mineral ions (e.g., Ca^{2+}, Mg^{2+}, Ba^{2+}, SO_4^{2-}, and CO_3^{2-}) to prevent scale formation in equipment and the oil and gas formations, but significant concentrations of monovalent ions (e.g., Na^+ and Cl^-) are often necessary for production. This requires high selectivity between monovalent and divalent ions by desalination membranes.

Current wastewater treatment strategies focus on minimizing contamination of the environment, and increasingly, extracting water for beneficial reuse. A more forward-looking approach is closed loop wastewater management that takes into consideration the economic benefits of high value chemicals in wastewater. Alkali (Li^+, K^+) and noble metals (Pt, Au) in seawater brine [24], nutrients (N and P species) in municipal wastewater, and a large variety of valuable chemicals including noble metals, alkali metals, rare earth elements (REEs) [18,25–27], nutrients, and valuable organics (e.g. pesticides, phenol, chloroform) in industrial wastewaters are highly attractive resources that can be recovered using membrane processes. For example, NF membranes with high permselectivity for monovalent over multivalent ions [16,28] could be used for recovering alkali metals (Li^+, K^+) and NO_3^- from waste brines. Selectivity among ions with the same valence and similar sizes could also be achieved using novel IEMs and LMs driven by electric field or concentration gradient [29]. Examples include selective H^+ transport over Na^+ in microbial electrochemical systems [30] and selective extraction of Li^+ over Na^+ from seawater and fresh surface waters [31].

Selectivity in conventional water treatment membranes

Selectivity-permeability trade-off

In any membrane separation processes, selectivity between two chemicals depends on their relative permeability through the membrane. For water treatment, high water permeability is desired to minimize energy consumption and membrane area needed, and high selectivity (i.e., high retention of contaminants) is necessary to ensure treated water quality. However, a trade-off between permeability and selectivity exists in most membrane materials, i.e., increasing permeability leads to a decrease in selectivity. The selectivity-permeability trade-off was first discovered in gas separation membranes [32]. The selectivity-permeability upper-bound of membrane materials was reported in 1991 for six gases, and was updated in 2008, serving as a benchmark for evaluating membrane materials. The same selectivity-permeability trade-off was also found in other synthetic membranes, including RO [33,34] (Fig. 2a), NF [35] (Fig. 2b), UF [36] (Fig. 2c), IEMs [37], (Fig. 2d), and FO membranes [38]. A recent study analysed more than 300 published papers on NF and RO membranes, and reported an upper limit of water permeability of 5 L $m^{-2}h^{-1}$ bar^{-1} in RO membranes for 99.5% salt rejection in seawater desalination [33]. Nevertheless, breaking the selectivity-permeability trade-off has been the aspiration and main objective of much membrane material research.

Selectivity of existing membrane materials

Membrane processes used for water and wastewater treatment utilize different driving forces, including hydraulic pressure, electric potential, and heat; each involves different mechanisms of selectivity.

Pressure-driven membranes. Pressure-driven membrane processes include MF, UF, NF, and RO, in the order of decreasing water permeability and increasing hydraulic pressure needed to drive the process.

RO membranes are considered dense non-porous membranes that separate water and solutes by size exclusion and Donnan effects (electric repulsion between a charged solute and similarly charged membrane). Chemical transport through RO membranes is commonly described using the solution-diffusion model: water or solutes are absorbed in and diffuse through the polyamide active layer. The membrane's selectivity between a solute and water is therefore determined by its difference in solubility and diffusivity in the active layer. State-of-the-art commercial polyamide RO membranes have water permeability of 2–3 L m^{-2} h^{-1} bar^{-1} with salt rejection over 99.5% [39–40]. Such excellent performance and the decreasing cost of RO membranes have resulted in the rapid increase in installation of seawater RO plants [41]. However, current RO membranes exhibit insufficient rejection of neutral, low molecular weight contaminants such as urea, ammonia (NH_3), boron (boric acid at natural water pH), 1,4-dioxane and NDMA. For example, boron rejection by seawater RO membranes is about 80%; this is insufficient to reduce boron concentration in seawater (typically 4.5–6 ppm) to the satisfactory level for irrigation (0.5 ppm) [42].

Compared with RO membranes, NF membranes are less dense, with an average pore diameter of 1 nm, corresponding to a molecular weight cut-off (MWCO) of 300–500 Da [43]. Separation is achieved by size exclusion and interactions between the membrane surface or pore wall and solute/solvent molecules, including the Donnan effect, dielectric effect, and hydrophobic interaction. Unlike RO membranes, which retain almost all salts, commercial piperazine-based or aromatic polyamide NF membranes have high rejection for multivalent ions (>90%), but relatively low retention (30–60%) of monovalent salts [44]. Thus, they are often utilized for water softening. NF membranes also have high rejection (>90%) for synthetic organic contaminants including pharmaceuticals, health supplements, and chemicals in personal care products such as cosmetics and perfumes [45]. Nevertheless, the selectivity for monovalent ions over multivalent ions or between organic chemicals is not high enough, limiting application for multivalent ion removal, valuable monovalent ion recovery, and target chemical separation.

The UF process uses membranes with pore sizes ranging from 2 to 100 nm, whose main separation mechanism is size exclusion. Thus, the selectivity of UF membranes is determined by membrane pore size relative to those of the chemicals. Polymeric UF membranes, such as poly(ether)sulfone, cellulose, and polyacrylonitrile, are usually prepared by phase inversion, which results in an approximately normal distribution of pore sizes. The narrower the pore size distribution is, the higher is the membrane selectivity. Because UF membranes separate chemicals by size exclusion, they have little selectivity between solutes of sim-

TABLE 1

Advanced materials used in different membrane types for selectivity.

	2D laminar membrane & Isoporous membrane	Dense membrane	Biomimetic membrane
Selectivity	Selective for **water** or **small sized ions** over **bigger ions and molecules**	Selective for **ions** over **water, ions, and molecules** with size bigger, similar and even smaller than the target ions	Selective for **water** over **ions and other molecules** or for **ions** over **other ions and molecules**
Advanced materials	▪ 2D materials GO, TMDs, Mxenes ▪ Isoporous materials porous graphene, vertically aligned CNTs, MOFs, COFs, LC polymers	▪ IEM coatings PSS, PAH, PEI, HACC, PANI, PEI, etc. ▪ LM extractants LIX 84-I, LIX 64N, DEHPA, PC88A, Cyanex 272, etc.	▪ Water channels aquaporins, macrocycles, imidazole-quartet, etc. ▪ Ion channels KcsA, POF, crown ether, pillararene-cyclodextrin, etc.

ilar sizes. Similar to UF, MF membranes (pore size 0.1–2.0 μm) retain particles by size exclusion; they only reject large suspended particles and have no selectivity between particles of similar sizes.

Ion exchange membranes. Ion exchange membranes are used in electrodialysis or electrodialysis reversal (EDR) processes, which utilize an electric field to separate ions from water. Driven by Coulomb force in an electric field, electrolyte ions transport through IEMs containing opposite charges. Cation exchange membranes (CEMs) have negative fixed charges and are permeable only to cations, while anion exchange membranes (AEMs) have positive fixed charges and allow only anions to pass [46]. Both CEMs and AEMs have high permselectivity for counter ions, with a transport number (fraction of the current carried by counter ions) reaching >0.98 in commercial IEMs [47]. However, a trade-off between cation/anion selectivity and membrane ionic resistance also exists in IEMs (Fig. 2d). The membrane ionic resistance is mainly determined by charge density and water content, which are important limitations of existing IEMs. In addition to selectivity between cations and anions, commercial AEMs also have high permselectivity for monovalent ions over multivalent ions. The permselectivity ($S_{i/j}$) between target species i and competitive species j in water-related membranes is normally defined as

$$S_{i/j} = \frac{J_i/C_{i,feed}}{J_j/C_{j,feed}} \quad (1)$$

where J_i and J_j are the flux of i and j across the membrane, respectively; $C_{i,feed}$ and $C_{j,feed}$ are the concentration of species i and j in the feed solution, respectively. In general, current IEMs exhibit no to low permselectivity between ions of similar valence, but higher permeability for monovalent than multivalent ions. For example, the Excellion I-200 membrane has permselectivity of 200–556 for ClO_4^-, NO_3^-, BrO_3^-, and $H_2PO_4^-$ over SO_4^{2-} and HPO_4^{2-}, and the Neosepta ACS membrane has permselectivity of $>10^4$ for these monovalent anions over SO_4^{2-} and HPO_4^{2-} [48]. Permselectivity for monovalent over multivalent cations is normally <10 in commercial CEMs [49,50].

Membrane distillation. An emerging desalination technology, MD is a hybrid, thermally driven membrane process. Feed water evaporates at the water–air interface formed at the pore opening of the hydrophobic microporous MD membrane. A transmembrane vapor pressure difference resulting from a temperature difference between the two sides of the membrane drives water vapor transport through the membrane, which condenses on the permeate side to form pure water, leaving solutes on the feed side [51,52]. MD can retain 100% of non-volatile solutes and the rejection is not affected by salt concentration [53] (Fig. 2e). However, volatile and semi-volatile substances, such as volatile organic compounds that are commonly present in oil- and gas-produced water, can transport through the membrane, compromising treated water quality [54]. In addition, low surface tension feed waters or membrane fouling and scaling can lead to wetting of membrane pores, drastically decreasing salt rejection. The selectivity in MD depends primarily on chemical volatility. It is only recently that selectivity among volatile compounds (e.g., VOC removal from water) has been brought to attention. Therefore, selective MD membranes are not discussed in this review.

Advanced materials in selective membranes

The demand for energy-efficient water treatment as well as the limitation in selectivity of existing membranes has motivated the pursuit of membranes that can break the selectivity-permeability trade-off and provide high selectivity for chemicals of interest. Significant research has been devoted to modifying existing membrane materials or developing novel membranes using advanced materials (Table 1). Bottom-up approaches are used to construct membranes with well-defined pore sizes and structures using novel building blocks, including two-dimensional nanomaterials, vertically aligned CNTs, metal/cova-

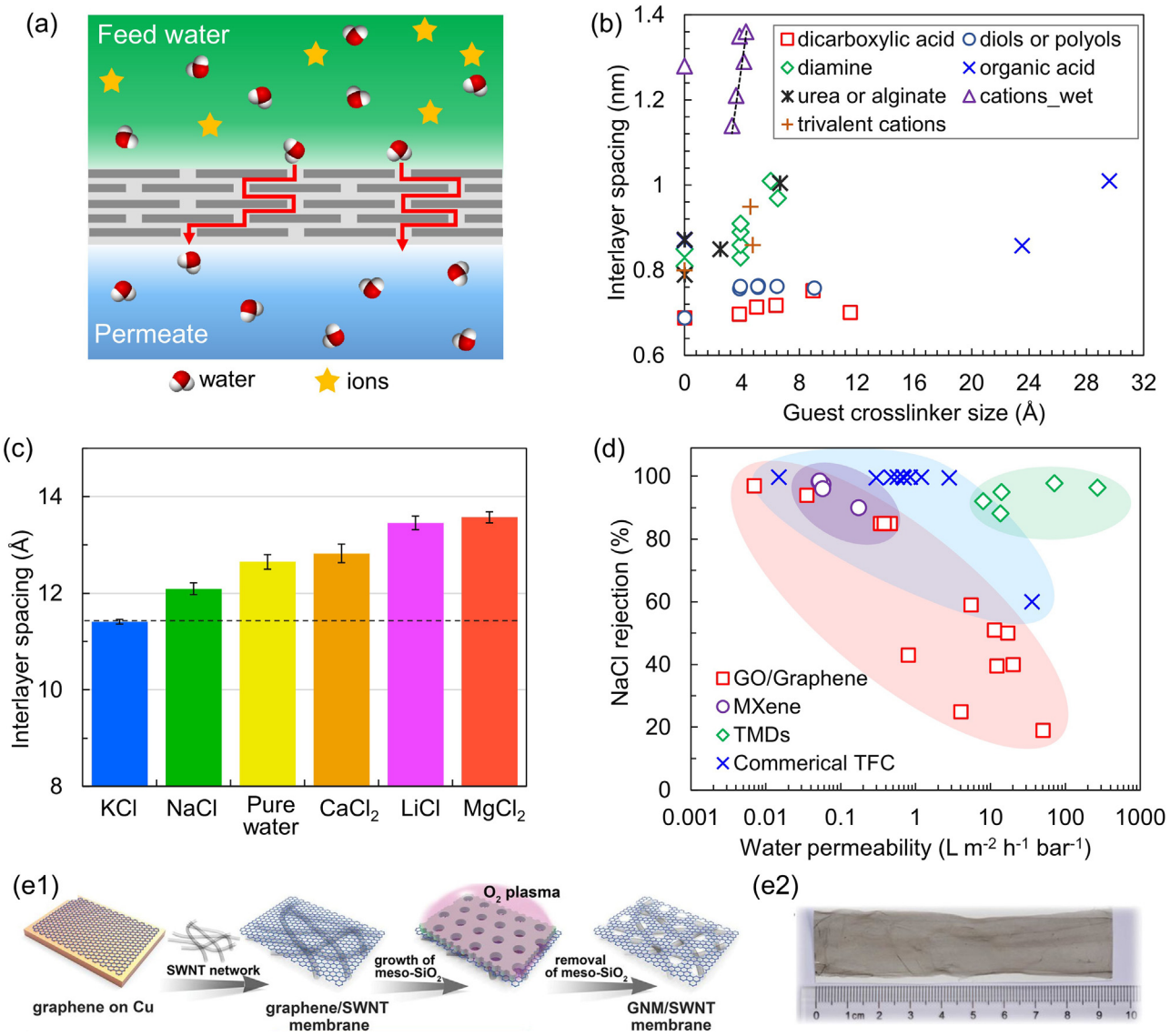

FIGURE 3

Performance of 2D laminar membranes fabricated by GO, TMDs, and MXene. (a) Schematic of 2D laminar membrane and transport through interlayer nanochannels; (b) Interlayer spacing of GO membranes cross-linked using different guest linkers. Data used in the Figure can be found in Table S1; (c) Interlayer spacings of a GO membrane that is pre-soaked in KCl solution, and then immersed in different solutions. Reproduced with permission from Ref. [141], copyright © 2017, Nature Publishing Group; (d) NaCl rejection and water permeability for commercial TFC membranes and laminar membranes made of GOs, TMDs, and MXenes. Data used in the figure is reproduced from Ref. [128] and can be found in Table S2; (e1) Schematic illustration of the process used to fabricate the single-walled carbon nanotubes (SWNTs) supported graphene nanomesh (GNM) hybrid membranes; (e2) Photograph of a large GNM/SWNT membrane (left) and a coupon of GNM/SWNT membrane supporting six coins. Scale bars: 1 cm. Reproduced with permission from Ref. [142], copyright © 2019, American Association for the Advancement of Science.

lent organic frameworks (MOFs/COFs), and liquid crystal (LC) polymers; unique chemistries are utilized to develop coatings and extractants for IEMs and LMs to increase the permselectivity of target ions or molecules; biological water and ion channels and their synthetic equivalents are incorporated in membranes to achieve highly selective water or chemical transport.

Membranes with precise pore sizes

Well-defined membrane pores with precise sizes can achieve high selectivity based on molecular/ion sizes. Membranes formed by assembling 2D nanomaterials into a laminar structure, by using isoporous network materials, i.e., MOFs and COFs, by vertically aligning CNTs, or by generating precisely sized pores in a graphene sheet have much narrower, more precise and tuneable pore size distribution than conventional membrane materials. The structure and thickness of the porous network dictate the transport pathway of permeants and hence permeability. In 2D laminar membranes, the sub-nanometer-sized channels between the laminae and the edge-to-edge defects or gaps between neighbouring 2D nanosheets [90] (Fig. 3a) allow passage of water and chemicals smaller than the channel size both along and perpendicular to the 2D plane while excluding larger species. In isoporous membranes (Fig. 4a), water and target solutes transport through the isoporous network formed by building blocks such

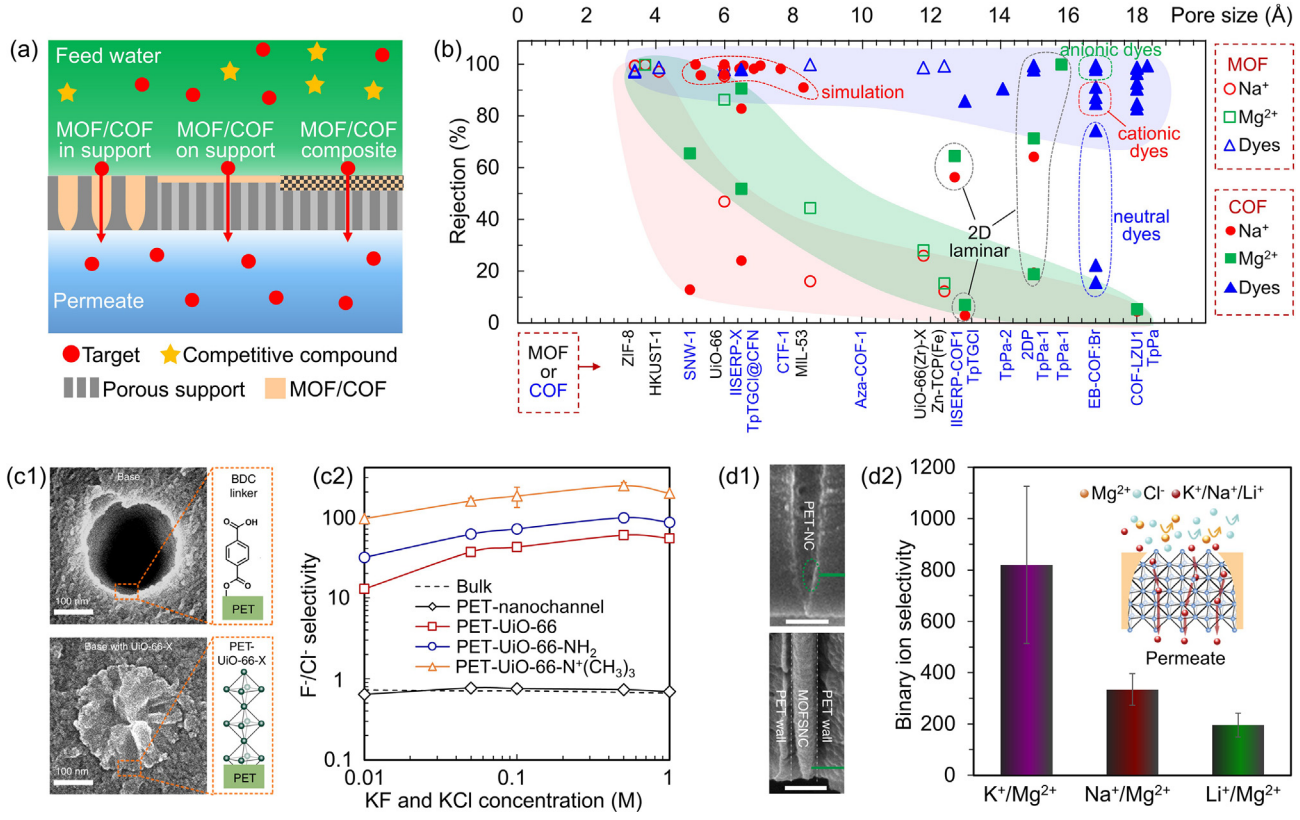

FIGURE 4

Isoporous membrane for water treatment. (a) Schematic of typical isoporous membranes: MOF/COF grown inside the pores or on the surface of a porous support, MOF/COF composites; (b) Pore size, rejection of Na^+, Mg^{2+}, and organic dyes of MOFs and COFs membranes. The light pink, green, and blue shaded areas represent the general rejection performance of MOF/COF membranes for Na^+, Mg^{2+}, and dyes, respectively. The charge of the dyes tested using the charged EB-COF:Br COF is marked. Data used in the Figure can be found in Table S3; (c1) SEM image of a polyethylene terephthalate (PET) nanochannel before (top) and after MOF growth; (c2) Selectivity of F^- over Cl^- by PET-UiO-66 MOF with various functional groups. Reproduced with permission from Ref. [159], copyright © 2020, Nature Publishing Group; (d1) SEM image of the polyethylene terephthalate (PET) nanochannel (NC) tip region before (top) and after (bottom) the growth of MOF UiO-66-$(COOH)_2$. Scale bar, 500 nm; (d2) Binary K^+/Mg^{2+}, Na^+/Mg^{2+} and Li^+/Mg^{2+} selectivity of the MOFSNC, with inset showing schematic of the binary ion permeation process. The concentration of all species in the binary concentration is 1 M. Reproduced with permission from Ref. [161], copyright © 2020, Nature Publishing Group.

as MOFs, COFs, porous graphene, vertically aligned CNTs and LC polymers, realizing fast and selective permeation of the target compounds.

2D nanomaterials for laminar membranes

The discovery that water molecules transport in a single layer at high speed in the nano-channels formed between two GO layers generated tremendous excitement about laminar membranes assembled from two-dimensional (2D) nanomaterials, including GO [91–92], TMDs, and MXenes [93–95]. Because 2D nanomaterials disperse well in solvents, these laminar membranes can be prepared using scalable, solution-based processes such as vacuum filtration [96–99], drop casting [99], and spin-coating [100–101]. The laminar structure and the diverse chemical functionalities available allow tuning of the membrane pore (i.e., interlayer nano-channel) size and length, as well as the pore wall surface chemistry and hence interactions with the solutes [102–105], allowing more precise control of membrane permselectivity.

GO membranes. One of the most important derivatives of graphene [106], GO is a single carbon layer with oxygen-containing functional groups including hydroxyl, carboxyl, epoxide, and carbonyl [107]. These oxygen-containing functional groups improve the dispersibility of GO in water, which is conducive to GO stacking to form laminar membranes. They also help form nanocapillaries between GO layers, allowing nearly frictionless flow of monolayer water in the pristine (unoxidized) regions [92,108]. Simulations suggest that an ideal water-permselective membrane should have an interlayer spacing of ~6 Å [92] to allow only one layer of water molecules to pass. However, when immersed in water, the interlayer spacing of GO membrane can grow to 10.5–14 Å [90,92,108]. Considering the thickness of the graphene basal plane (~3.5 Å) [109], the transport channel height, 7–10 Å (Fig. 3b), is too large to achieve high salt ion rejection even though it allows fast permeation of multilayer (>2 layers) water molecules [92]. Furthermore, the oxygen-containing functional groups can interact with water to form hydrogen bond [107], leading to membrane swelling and even disassembly of GO nanosheets [110,111].

The selectivity and stability of GO laminar membranes can be improved by partial removal of oxygen-containing functional groups using chemical reduction [112,113], thermal treatment [114], ultraviolet irradiation [115], and electrochemical reduction

[116], to form reduced GO (rGO) membranes. Removing oxygen-containing functional groups limits the hydration effect and reduces the interlayer spacing to 3.5–5.0 Å [98,117–119], achieving NaCl rejection of 40–81.7% [98,118,119]. Another approach to adjusting the interlayer spacing and enhance membrane stability is cross-linking GO layers using guest molecules, including dicarboxylic acids [103], diols or polyols [103], urea [120], diamines [121,122], larger organic acids such as alginic [123] and tannic acids [124], polymers [104,125], and metal cations with various valences [102,126] (Fig. 3b, Table S1). The insertion of crosslinkers causes a slight increase in interlayer spacing compared to pristine GO membranes. Nevertheless, the interlayer spacing is not necessarily consistent with the length of the crosslinker (Fig. 3b, Table S1). For example, crosslinking using dicarboxylic acids with chain length of 3.80 (oxalic acid), 8.94 (hexanedioic acid) and 11.54 Å (octanedioic acid) increased the GO membrane interlayer spacing from 6.89 (pristine) to 6.98, 7.53 and 7.02 Å, respectively [103]. Similar results were observed with diols and diamines. In general, the increase in interlayer spacing is much smaller than the change in organic crosslinker chain length (Fig. 3b), due to the dimensional heterogeneity of the crosslinker molecules and their different orientation between GO layers. In contrast, metal cations with a spherical geometry tunes the interlayer spacing much more precisely according to their sizes. A nearly perfect linear correlation was obtained between the interlayer spacing of a freestanding GO laminar membrane and the size of metal cations crosslinkers [102] (Fig. 3b). The interlayer spacing could be controlled within 0.1 nm of the hydrated cation size (Fig. 3c) [102] resulting in extremely high membrane selectivity by size. For example, the membrane crosslinked by K^+ realized 99% rejection of larger ions including Na^+, Mg^{2+}, and Ca^{2+}. However, the stability of the K^+ crosslinked membrane needs to be evaluated. Other ion crosslinkers also need to be tested to produce a wider range of interlayer spacings.

TMD and MXene membranes. TMDs are 2D nanomaterials consisting of a layer of transition metal atoms (e.g., Mo and W) sandwiched between two layers of chalcogen atoms (S, Se or Te) [127]. Without any oxygen-containing functional groups, TMD laminar membranes exhibit less swelling in aqueous solutions compared with GO membranes [128]. However, such reduced swelling also results in very small interlayer capillaries (~0.03 Å for bare MoS_2), blocking water transport. Functionalization of the TMD surface is therefore necessary to increase the width of the capillaries while limiting swelling. MoS_2 has been functionalized with organohalides, dyes, or other molecules, which expand the width of the interlayer capillaries to 4.5–5.4 Å, achieving >95% NaCl rejection [128,129]. Without the strong interactions between the oxygen functional groups and water, water permeability of TMD membranes could reach 75–322 L $m^{-2}h^{-1}$ bar^{-1} [129–132], two to five times higher than GO laminar membranes and one to two orders of magnitude higher than commercial TFC membranes with similar salt rejection (Fig. 3d, Table S2). In addition, TMD membranes have excellent structural stability: the interlayer spacing does not change in various solvents; continuous operation for more than six months showed no loss in salt rejection [129].

Another group of 2D nanomaterials that has been explored as membrane materials are MXenes. MXenes are 2D transition metal carbides, nitrides or carbonitrides produced from etching the A layer of bulk MAX to form layered $M_{n+1}X_nT_x$ [133,134], where M is a transition metal, A is an A-group (Groups 13 and 14) element, X is carbon or nitrogen atoms, and T is the surface terminal group (e.g., O, –OH, -F). The surface terminal groups provide the hydrophilicity necessary for MXene dispersion during membrane fabrication, but lead to swelling and hence poor rejection of monovalent cations similar to that in GO membranes [135,136]. Strategies such as chemical cross-linking can be used to control swelling and achieve high salt rejection. High monovalent ion rejection (>98%) and long term stability (70–400 h) have been achieved by either Al^{3+} intercalation [137] or self-crosslinking through reactions between oxygen-containing groups (–OH + –OH = –O– + H_2O) [138], forming relatively small interlayer spacing and consequently high salt rejection.

In addition to different surface chemistry, which results in difference in hydrophilicity, swelling properties, and water transport behaviours among GO, MXene and TMD membranes, these 2D nanomaterials also have distinct thickness (GOs < TMDs < MXenes) and nanosheet size (GO > TMDs ≈ MXenes). The large plane size-to-thickness ratio of GO enables fabricating laminar membrane with fewer pinholes compared with TMDs and MXenes, which may improve membrane selectivity but may also cause decrease of permeability. The smaller plane size of TMDs and MXenes also results in weaker interlock between nanosheets and hence lower robustness than GO. In addition, MXenes have higher electrical conductivity than GO and TMD [136], which may also affect their charge-based selectivity and application scenarios in water treatment. These 2D nanomaterials have great potential for laminar membranes with high water permeability and tuneable rejection of solutes. Nevertheless, fabricating defect-free laminar membranes with well-aligned nanosheets is challenging [139]. Acquiring these nanosheets such as MoS_2 and WS_2 from their bulk materials using the liquid-phase exfoliation method also has low yields and is time-consuming [140].

Single layer porous graphene and vertically aligned CNT membranes

Membranes with short and straight pores of precise and uniform sizes are ideal for separation. Creating uniform pores on graphene sheets or vertically aligning CNTs provides potential membrane materials with these properties.

Single layer porous graphene. Considering its single-atom thickness, creating high density pores of precise sizes on a single layer of the 2D graphene sheet would in theory yield the ultimate combination of permeability and selectivity. Simulations predict that such single-layer nanoporous graphene, with pore size <0.55 nm, could achieve two to three orders of magnitude higher water flux than existing RO membranes while maintaining high salt rejection [60]. Researchers have tried to produce sub-nanometer pores in graphene, and the best results were obtained using oxygen plasma. Direct treatment of single layer graphene using oxygen plasma produced pore size of 0.5–1.0 nm with pore density of 10^{12} pores cm^{-2} [143]. These pores are smaller than or similar to the size of salt ions in water, and

could reject nearly 100% of salt ions while producing a water flux of 252 L m^{-2} h^{-1} bar^{-1}.

A critical challenge in this approach is the difficulty in fabricating large-scale, mechanically robust single layer porous graphene membranes. A recent study demonstrated success in producing a large (2.0 cm × 9.5 cm), free-standing graphene-nanomesh/single-walled CNT (GNM/SWCNT) hybrid membrane (Fig. 3e) [142]. The single layer graphene membrane was supported by a SWCNT network, and high density, uniform, sub-nanometer pores were generated by oxygen plasma etching with a mesoporous SiO_2 mask. With plasma etching time of five and ten seconds, the membranes exhibited water permeability of 7.5 and 20.6 L $m^{-2}h^{-1}$ bar^{-1}, respectively, 85.2 to 93.4% ion rejection (with the order of KCl < NaCl < $MgCl_2$ < Na_2SO_4), and excellent mechanical strength. Nevertheless, single layer porous graphene membranes suitable for practical applications remain unachievable due to the limited plane size.

Vertically aligned CNTs. Carbon nanotubes, with atomically smooth and non-polar surfaces, offer exceptional pore space for water transport. Molecular dynamic simulation has predicted that single-walled (6,6) CNTs with an inner pore diameter of 0.47 nm can fully reject salt ions and realize a water permeability of 23 water molecule $tube^{-1}$ ns^{-1} [144,145]. At a CNT density of 1.0 × 10^{13} cm^{-2}, vertically aligned CNT (VACNT, 0.81 nm in CNT diameter) membranes could provide a water permeability of 3,096 L $m^{-2}h^{-1}$ bar^{-1} with salt rejection of >97% [144].

Despite the excellent performance predicted by model simulations, VACNT membranes have not shown the anticipated superior water permeability and salt rejection. Because the interior pore size of CNTs is significantly larger than the sizes of monovalent ions, VACNT membranes cannot be directly utilized for desalination. Synthesizing CNTs with sub-nanometer interior pore size is extremely challenging. Therefore, VACNT membranes are more suitable for ultrafiltration or nanofiltration applications. Density of CNTs has increased from 10^{10} to 10^{11} cm^{-2} in earlier VACNT membranes [146,147] to 1.3–3 × 10^{13} cm^{-2}, improving water permeability by one to two orders of magnitude (2070–10,500 L $m^{-2}h^{-1}$ bar^{-1}) [148,149]. Utilizing the interstitial pore space between CNTs could further improve membrane permeability [150].

MOFs and COFs

Metal organic frameworks (MOFs) and covalent organic frameworks (COFs) are isoporous materials formed by precise assembly of building block molecules, creating a structure of periodic skeletons and ordered pores. MOFs are comprised of metal ions/clusters linked by organic moieties [151], while COFs are crystalline organics with building blocks assembled in a periodic porous structure via covalent bonds [152,153]. Both have high porosity, tuneable pore sizes, well-defined pore structure, and adjustable surface chemistry, making them appealing candidates as separation membranes [154]. MOFs and COFs can be synthesized in membranes with various structures (Fig. 4a) using different strategies. For example, in situ growth by immersing a porous support in the precursor solution could form continuous MOF/COF membrane on the porous support surface or grow MOF/COF inside the pores of the support. Adding MOF/COF powders to the membrane polymer casting solution could form mixed matrix membranes.

MOFs/COFs-based membranes possess two major advantages: (i) the uniform pore size in MOFs/COFs can precisely exclude molecules and ions larger than the pore size, presenting excellent selectivity; (ii) the unique pore geometry combined with precise, tuneable pore size and rich chemical functionality in MOFs/COFs provide multiple mechanisms for selectivity among chemicals.

MOFs. With a precise porous crystalline structure, the selectivity of MOFs is mainly realized by size exclusion. The pore diameter of MOFs ranges from 0.3 to 2.0 nm [155]. This covers the pore size range of RO and NF membranes and can be utilized for desalination and organics removal. Fig. 4b shows the pore sizes of common water-stable MOFs: ZIF-8 [156,157], HKUST-1 [155], UiO-66 [158], MIL-53 [155], and their derivatives. ZIF-8, one of the most effective and reliable MOFs reported for water desalination, has 99.5% rejection for Na^+, Mg^{2+}, and organic dyes due to the small pore size (3.4 Å). HKUST-1, with a pore diameter of 4.1 Å, also exhibits high rejection of salt ions and organic dyes (Fig. 4b). Ion rejection decreases significantly for MOFs of larger pore sizes. Dynamic changes in ligand coordination mode, and defects in the MOF crystals due to missing ligands [158] also contribute to the decreased rejection. For example, MOF UiO-66 has a pore size smaller than the sizes of hydrated salt ions, but its salt rejection is relatively low (Fig. 4b).

In addition to the size exclusion mechanism that enables high selectivity for water, specific interactions between ions/-molecules and active adsorption sites in MOFs lead to selective absorption, resulting in high permselectivity of a target solute over other species with similar sizes. Zirconium-based MOF UiO-66-X (X = H, NH_2, and $N^+(CH_3)_3$) crystals grown in polyethylene terephthalate nanochannels (PET-NCs) [159] (Fig. 4c) exhibited ultrahigh F^- permselectivity ($F^- \gg Cl^- > Br^- > I^- > NO_3^- > SO_4^{2-}$) under an electric field. The selectivity for F^- over Cl^- reached ~240 with the UiO-66-$N^+(CH_3)_3$ membrane, rivaling biological and synthetic fluoride ion channels [160]. The ultrahigh selectivity originates from the strong interaction between F^- and Zr sites. Similar interactions may be utilized for selective transport of other ions. In another study, carboxylic groups on 3D porous UiO-66-$(COOH)_2$ grown in polyethylene terephthalate nanochannels [161] were found to cause partial dehydration of hydrated cations during their transport in the modified MOF channels, leading to different conductivity, mobility, and concentration in MOF nanochannels (Fig. 4d). Although the carboxylic groups have higher binding affinity for divalent (Ca^{2+}, Mg^{2+}) than monovalent cations (Li^+, Na^+, K^+), the permeability of monovalent ions was three orders of magnitude higher than that of divalent ions due to their much lower dehydration energy.

COFs. Several recent reviews have thoroughly discussed the synthesis and properties of COFs as well as their assembly into membranes and application for water treatment [152,154,162–165]. Compared with MOFs, COFs possess greater structural and chemical stability in aqueous solutions, but larger pore sizes (0.5 to 4.7 nm) (Fig. 4b). Although not able to retain salt ions, these large pores can be used in nanofiltration and ultrafiltration processes to remove dyes and other organic molecules. A TpPa

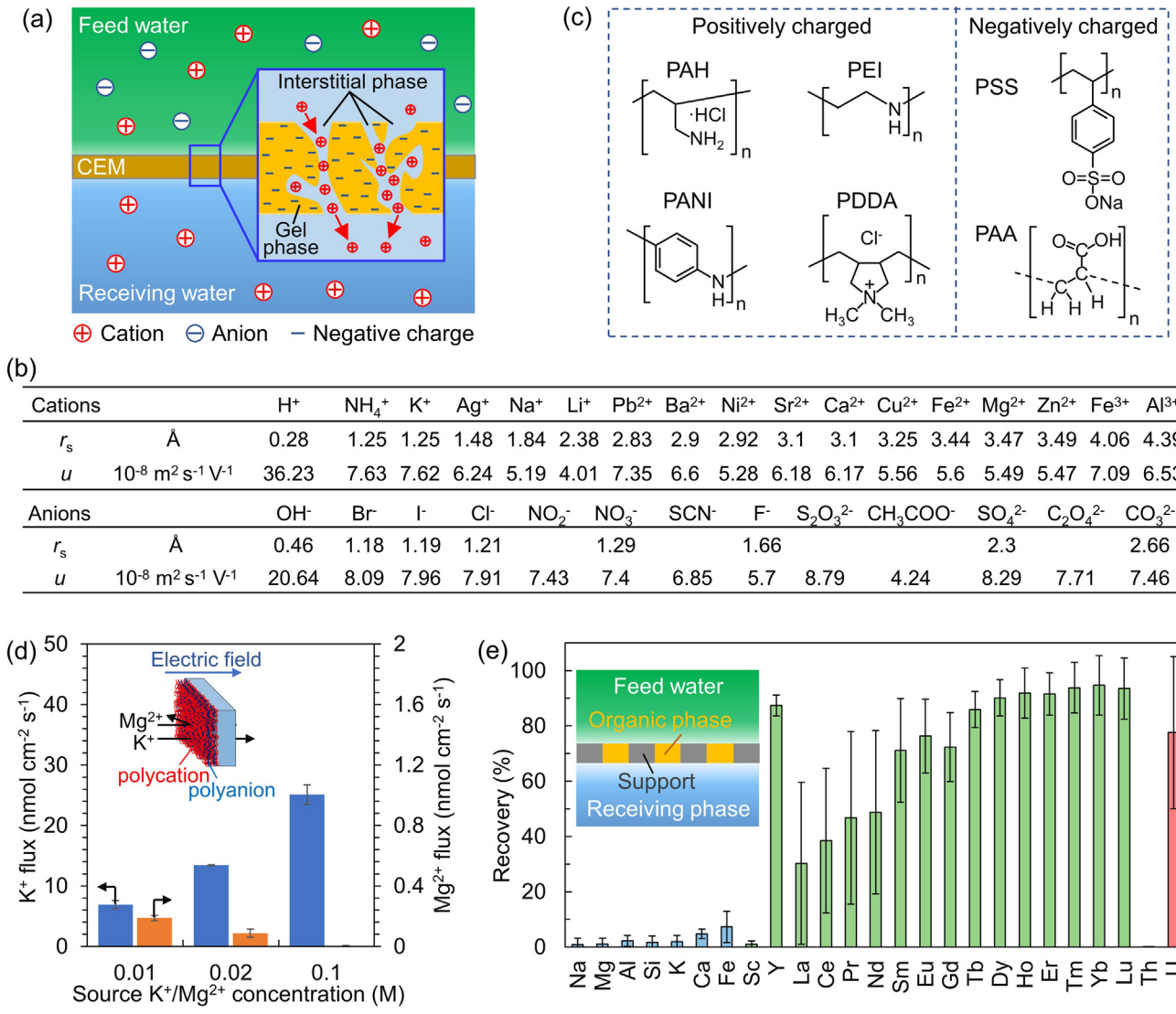

(b)

Cations		H^+	NH_4^+	K^+	Ag^+	Na^+	Li^+	Pb^{2+}	Ba^{2+}	Ni^{2+}	Sr^{2+}	Ca^{2+}	Cu^{2+}	Fe^{2+}	Mg^{2+}	Zn^{2+}	Fe^{3+}	Al^{3+}
r_s	Å	0.28	1.25	1.25	1.48	1.84	2.38	2.83	2.9	2.92	3.1	3.1	3.25	3.44	3.47	3.49	4.06	4.39
u	10^{-8} m^2 s^{-1} V^{-1}	36.23	7.63	7.62	6.24	5.19	4.01	7.35	6.6	5.28	6.18	6.17	5.56	5.6	5.49	5.47	7.09	6.53

Anions		OH^-	Br^-	I^-	Cl^-	NO_2^-	NO_3^-	SCN^-	F^-	$S_2O_3^{2-}$	CH_3COO^-	SO_4^{2-}	$C_2O_4^{2-}$	CO_3^{2-}
r_s	Å	0.46	1.18	1.19	1.21		1.29		1.66			2.3		2.66
u	10^{-8} m^2 s^{-1} V^{-1}	20.64	8.09	7.96	7.91	7.43	7.4	6.85	5.7	8.79	4.24	8.29	7.71	7.46

FIGURE 5

Selectivity in IEMs and LMs. (a) Two-phase structure model in IEMs; (b) Stokes radius (r_s) and electrophoretic mobility (u) of cations and anions in aqueous solution at 25 °C (adapted from Ref. [16] and reproduced with permission of copyright © 2018 Elsevier B.V.); (c) Commonly used positively and negatively charged polymer coatings. (d) K^+ and Mg^{2+} fluxes as a function of applied current density in 2-cell ED experiments using Nafion 115 membranes coated with a layer-by-layer assembled PSS/PAH multilayer. Adapted from Ref. [215] and reproduced with permission of copyright © 2015 American Chemical Society; (e) Average percent recovery of major elements and REEs from a leachate of coal fly ash via SLM using 10% DEHPA in kerosene after 24 h. Insert is a schematic of supported liquid membrane. Adapted from Ref. [17] and reproduced with permission of copyright © 2019 American Chemical Society.

COF membrane formed by interfacial polymerization realized 99.5% Congo red rejection and water permeability of 50 L m^2 h^{-1} bar^{-1} [166]. Different types of TpPa COFs [167–173] and other COFs, including COF-LZU1 [174] and TpTGCl [175], have been used in membranes (Table S3), and demonstrated dye rejection greater than 90%.

The tuneable chemistry of COFs allows grafting of charged functional groups, enabling rejection of charge species by Donnan exclusion. A membrane fabricated by layer-by-layer assembly of a quaternary amine-functionalized 2D cationic COF achieved greater than 84 and 98% rejection of cationic and anionic dyes, respectively, despite its low rejection for neutral dyes. It also exhibited a very high water permeability of 546 L m^{-2}h^{-1} bar^{-1} [105]. Many attempts have been made to develop salt-rejecting COF membranes, although a NaCl rejection of >90% has not been achieved. Functionalizing COF pores to reduce the pore size has been predicted to achieve >95% NaCl rejection (Fig. 4b) [176,177]. By introducing –COOH groups in the hexagonal pores, the pore diameter of IISERP-COF1 was reduced from 1.27 to 0.65 nm, increasing NaCl and $MgCl_2$ rejection from 56.4 and 64.6% to 82.9 and 90.6%, respectively [178] (Fig. 4b). Similarly, changing the pendant group from hydrogen to ethyl in an polyacrylonitrile-supported COF (TAPB-PDA-H) membrane reduced the pore diameter from 3.4 to 3.2 nm, leading to an increase in NaCl rejection from 17.1 to 33.9% despite that the pores were still much larger than hydrated Na^+ or Cl^- [179]. In addition, two-dimensional COFs have been synthesized and used to form laminar membranes. The interlayer spacing provides another water transport path and can be tuned to achieve ion rejection. Reducing the interlayer spacing of 2D laminar COF (TpPa-1 [172], COF-1 [180], 2DP [169]) membranes to 0.3–0.9 nm achieved NaCl rejection of 7.6–64.3% (Fig. 4b), even

though their in-plane pore size (13–15 Å) is much larger than that of Na^+ (7.2 Å).

Creating scalable and stable membranes is critical to the success of MOFs/COFs as selective membrane materials. A promising strategy is in situ growth of MOFs/COFs in the pores of large-pore-size membranes [159,161] or on the surface of large-scale porous substrate [158] (Fig. 4a). 2D MOFs and COFs can form laminar membranes, which can be stabilized by cross-linking with proper linkers [181,182]. In addition, because the organic nature of MOFs/COFs makes them more compatible with membrane polymers than inorganic nanomaterials, fabricating mixed matrix membranes by blending MOFs and COFs with conventional membrane polymers has shown success in many studies [165,183]. A MOF/COF active layer can also be formed in thin film nanocomposite membranes through interfacial polymerization [166,184]. Alternatively, GO/COFs hybrid membrane could be synthesized by intercalating COF nanoparticles into laminar GO membranes, achieving high water/organic solute permeability while maintaining superior organic dye rejection rate [185].

Liquid crystal polymers

Lyotropic liquid crystals (LCs) are amphiphilic molecules containing a hydrophobic organic tail section and a hydrophilic headgroup [186]. In the presence of immiscible liquid (e.g., water), LC molecules self-organize into ordered yet fluid assemblies containing 1D nanochannels, 2D-layered structures, or 3D bicontinuous networks [187,189], with the tails forming fused hydrophobic regions and the hydrophilic headgroups defines the interface. Such ordered structures distinguish LCs from conventional surfactants and lipids that only form discrete and disordered aggregates (e.g., normal or reverse micelles, vesicles, microtubules). After cross-linking by photo- or thermal- initiation processes to retain and stabilize the microstructures, LC polymers can form separation membranes with pore size ranging from sub-nanometer to over 10 nm [189,190], covering the pore size of conventional RO to UF membranes. The LC polymeric membranes possess several advantages [191]: (i) designable channels to give uniform and desired structure, which is the major advantage over conventional polymeric membranes in terms of selectivity as it allows the LC membrane to distinguish small size differences; (ii) possibility of forming defect-free films because the transformation of melt LC states into solid membranes can be initiated by in situ polymerization; and (iii) high number density of channels.

LC polymeric membranes have been utilized for water desalination and organic compounds removal. They utilize the same separation mechanisms as conventional NF/RO membranes: size exclusion and Donnan effects [189]. Contaminant rejection by LC membranes with uniform and fine pores is in generally similar to that of NF membranes, i.e., higher rejection for molecules or ions of larger size and higher charges, but water permeability of reported LC membranes is often lower than commercial NF membranes due to their significantly thicker active separation layer (several to tens of micrometers) [189,190]. Control of the thickness of the LC separating layer is important to enable high flux. Alignment of columnar LCs (e.g., using magnetic field) to form vertical pores spanning the active layer could also decrease channel tortuosity and improve water permeability.

Nevertheless, it is challenging to fabricate LC membranes mechanically robust enough to withstand the high pressure needed for filtration [189]. Utilizing a porous polymer support is a potential approach to achieve the necessary mechanical stability. Furthermore, more readily synthesized LC monomers and facile LC membrane fabrication methods are needed [186].

Dense membranes

IEMs and LMs are poreless or pore-filled membranes. Chemical transport through these membranes is driven by an electric and/or chemical potential, and is usually described by the solution-diffusion model. Because separation is not based on size exclusion, selectivity for target ions or molecules over those with similar or even smaller sizes is possible.

Ion exchange membranes

IEMs are dense membranes that bear fixed charges in the polymer matrix. The fixed charges allow selective permeation of counter-ions but reject similarly charged co-ions through the Donnan effect. Common polymers used in IEMs include poly(s tyrene-co-divinylbenzene), poly(propylene), and poly(ethylene). They are functionalized with anionic ($–COO^-$, $–SO_3^-$, $–PO_3^{2-}$, etc.) or cationic ($–NH_3^+$, $–NRH_2^+$, etc.) groups to form cation exchange (CEMs) or anion exchange (AEMs) membranes. IEMs have been widely utilized in industry processes such as ED [192,193], electrolysis [194], capacitive deionization (CDI) [195–198], microbial fuel cells [199–202], and batteries for water treatment, energy production, food, and medical processing.

A microstructure model consisting of a dense gel phase and an interstitial phase is often used to describe IEMs (Fig. 5a) [203]. The gel phase is the charged polymer network with hydrophilic ion-exchange functional groups on a polymer backbone; the interstitial phase is the free volume between polymer chains, which causes membrane swelling when filled with solution. The interstitial phase provides the transport channel for counter ions while the charges on the gel phase keep the co-ions out. When the size of interstitial phase exceeds 1.5 nm [204], the Donnan effect is weakened and passage of co-ions occurs, compromising IEM selectivity [205,206]. The volume of the interstitial phase is measured by the water content of a wet IEM. Commercial IEMs often have a water content of < 60% to ensure effective rejection of co-ions. Higher water content results in membrane swelling and compromises permselectivity for counter ions over co-ions [37].

Conventional IEMs also exhibit some permselectivity among counter-ions of different valence or size. The permselectivity is determined by the solubility and electrophoretic mobility of the ions in the membrane. Ion solubility in IEMs follows trends similar to those in conventional ion exchange resins: ions with higher valence, or of larger radius when the valence is the same, are preferentially exchanged [207–210]. For example, selectivity of sulfonic cation exchange resins follows the order of Ba^{2+} > Pb^{2+} > Sr^{2+} > Ca^{2+} > Mg^{2+} > Ag^+ > K^+ > NH^+ > Na^+ > Li^+, which increases with increasing ion valence and radius. On the other hand, electrophoretic mobility of ions inside the membrane increases with increasing valence, but decreases with the Stokes radius of the ions. The electrophoretic mobility of common ions

is compared in Fig. 5b. Overall, ion permselectivity of most commercial IEMs seems to be more consistent with the solubility order. For example, transport of common cations through CEMs with fixed sulfonic acid groups follows the order $Ba^{2+} > Pb^{2+} > Sr^{2+} > Ca^{2+} > Mg^{2+} > Ag^{+} > K^{+} > NH^{+} > Na^{+} > Li^{+}$. Most commercial IEMs have higher permselectivity for multivalent ions over monovalent ions.

In water treatment, high permselectivity for monovalent ions over multivalent ions is desired for scaling mitigation or recovery of valuable chemicals (e.g., Li^{+}, K^{+}). Efforts have been made to modify IEMs for higher monovalent ion permselectivity [211–214]. A commonly used approach is to increase transport resistance of multivalent ions by applying a dense coating layer with charges opposite to the fixed charges. The charged coating repels multivalent ions more strongly than monovalent ions [215–218], resulting in increased monovalent ion permselectivity. For CEMs, cationic polymers such as protonated polyaniline (PANI), poly-ethyleneimine (PEI), poly(allylamine hydrochloride) (PAH), hydroxylpropyl trimethyl ammonium chloride chitosan (HACC), poly(diallyldimethylammonium chloride) (PDADMAC), and quaternized chitosan have been utilized to hinder multivalent ion transport and enhance selective permeation of Li^{+}, Na^{+}, and K^{+} (Fig. 5c). Although fewer studies on monovalent selective AEM have been reported, surface modification using poly(styrene sulfonic acid) (PSS), polyacrylic acid (PAA), and other anionic or neutral organics, such as sodium naphthalene sulfonate and formaldehyde, have been shown to enhance permselectivity for Br^{-} and NO_3^{-} over SO_4^{2-} [217]. The Donnan effect is magnified in layer-by-layer (LBL) assembly of alternating cationic/anionic polyelectrolyte multilayer coatings, where the ions encounter a similarly charged polyelectrolyte layer multiple times, resulting in higher permselectivity (10^3–10^3) for monovalent over multivalent ions [219]. For example, CEM modified by PSS/PAH LBL multilayers showed K^{+}/Mg^{2+} selectivity >1000 [215,220,221] (Fig. 5d), Li^{+}/Co^{2+} selectivity >1000, and Li^{+}/La^{3+} selectivity >5000 [221]. A PSS/HACC-modified AEM achieved Cl^{-}/SO_4^{2-} selectivity of 2.9, much higher than that of the pristine AEM (0.66) [222]; an N-O-sulfonic acid benzyl chitosan (NSBC)/HACC LBL coating also improved the permselectivity of Cl^{-}/SO_4^{2-} from 0.81 to 47.04 [223].

Liquid membranes

LMs enable liquid–liquid extraction using a nonaqueous phase containing dissolved chelating or ion exchange agents as the membrane. When exposed to the feed water and a stripping solution on opposite sides of the LM, the target solutes dissolve into the LM, and are then released into the stripping solution. LMs combine the extraction and stripping processes into a single step, realizing continuous separation of target species using a small amount of organic solvent [224]. Based on configuration, LMs are classified as bulk liquid membranes (BLMs), emulsion liquid membranes (ELMs), and supported liquid membranes (SLMs) (the insert of Fig. 5e). BLMs use a bulk membrane phase to separate the aqueous feed and the stripping solution, whereas the stripping phase forms a stable emulsion in the ELMs. A SLM utilizes a microporous polymeric or inorganic film, which holds the

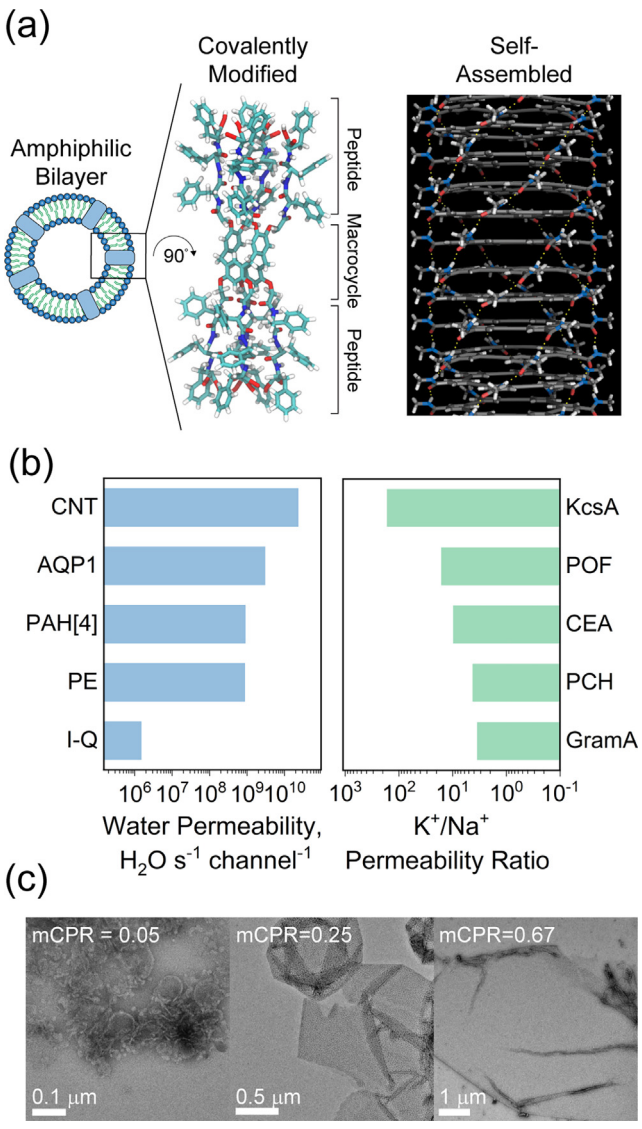

FIGURE 6

Selectivity and fabrication of biological and artificial channels for water treatment. (a) Macrocycles can be covalently modified or self-assembled to form artificial channels embedded in an amphiphilic bilayer (shown as a lipid vesicle). For covalent modification, a hybrid arene macrocycle appended with peptide chains is shown [244]. For self-assembly, a molecular dynamics snapshot of a stack of *m*-phenylene ethynylene macrocycles is shown. Hydrogen bonds are represented by dashed yellow lines. Channel images reproduced from Ref. [248], copyright © 2020, and Ref. [244], copyright © 2012, Nature Publishing Group. (b) Water permeability of channels that demonstrate water/salt selectivity: carbon nanotubes (CNT) [265], aquaporin-1 (AQP1) [266], peptide-appended hybrid [244] arenes (PAH) [248], *m*-phenylene ethynylene (PE) [244], and imidazole-quartet (I-Q) water channels [267] (left). K^{+}/Na^{+} permeability ratios of the KcsA K^{+} channel [268] and other artificial K^{+} channels constructed from pyridine/oxadiazole-based helical foldamer (POF) [259], a crown ether assembly (CEA) [258], pillararene-cyclodextrin hybrid (PCH) [257], and gramicidin A (GramA) channels (right). (c) Negative-stain transmission electron microscopy images showing molar channel-to-polymer ratios (mCPRs) of 0.05, 0.25, and 0.67 yield small vesicles, large vesicles, and flat crystalline sheets, respectively, using slow detergent dialysis. Images show PAP artificial water channels in a poly(butadiene)-b-poly(ethylene oxide) diblock polymer matrix [246]. Image adapted and reproduced from Ref. [247], copyright © 2018, Nature Publishing Group.

extractant in the pores. Although invented in the 1960s [225], LMs have not been intensively studied due to their poor stability. In recent years, interest in LMs has resumed owing to their very high selectivity among diverse ions and molecules, and the independence of such selectivity on solute size.

Solute transport in LMs is mainly determined by its partition in the membrane phase through complex formation and ion exchange [226]. Common metal chelating agents include LIX hydroxyoximes (LIX 84-I, LIX 64 N, LIX 62 N, LIX 860, etc.) and phosphoric acid derivatives such as DEHPA, PC88A, and Cyanex 272. These extractants can reach selectivity of $>10^3$ for Cu, Zn, Co, Ni, Fe, Mn, Mo, and REEs over common cations such as Na^+, K^+, Mg^{2+}, and Al^{3+} [17,18,227,228]. For example, an SLM containing 10 v% DEPHA in kerosene recovered 16 REEs from fly ash leachate with separation factors of 10^1–10^3 over Na, K, Mg, Fe, and Al (Fig. 5e); a large scale SLM with tributyl phosphate as the extractant and Isopar-L as the solvent recovered high purity (99.5 wt%) REEs from scrap permanent magnets with more than 95% recovery [227]. Metal oxyanions such as Mo, Cr, Co, and V are more commonly separated through the ion exchange mechanism using amine-based extractants including Aliquat-336 [229], Alamine-336 [230], and Alamine-304. Aliquat-336- based LMs were shown to extract Co^{2+} at 100% recovery from a mixed solution containing Ni^{2+} [231], and demonstrated very high Cr (VI) selectivity (231–6,000) over Cl(I), Pb(II), Al(III), Co(II), Ni (II), Cd (II), and Zn (II) [229,230].

A major barrier to the application of LMs is their low stability. Loss of organic extractants to the feed and/or receiving solution leads to short LM lifetime and pollution of the product stream. Currently, most SLMs are fabricated using hydrophobic polypropylene [18] and PVDF [224] hollow fiber membranes, which can be operated for 100 h with little performance decline. Adding plasticizers or using novel support materials and configurations can improve LM stability. For example, adding 2-nitrophenyl-octyl ether to [A336][SCN] extractant in a PVDF support demonstrated stable performance over nine days [232]; sandwiching the liquid organic phase between dense IEMs may improve the LM stability and allow its application in the ED process [233]. Furthermore, development of low-cost and environmentally friendly solvents such as sunflower oil [234] and mineral oil [17] could reduce the cost and safety risks of LMs; a strategy of regularly refilling the organic phase in LMs [235] helps maintain continuous operation. Regardless, improving LM stability remains a critical research need in order to take advantage of their unrivalled selectivity in practical water treatment applications.

Biological and artificial channels

Naturally occurring protein channels that are aligned in cell membranes provide an inspirational platform for water treatment membranes that possess high permeability and selectivity [236]. Remarkably, biological water channels known as aquaporin-1 (AQP1) allow permeation of 10^9 H_2O s^{-1} $channel^{-1}$ while also excluding solutes, including protons and small neutral solutes such as urea [237,238]. The KcsA K^+ channel, an ion-selective channel, is no less remarkable, maintaining permeability up to 10^8 ions per second and 10^4 K^+ ions transport for every Na^+ ion [239,240]. However, low protein stability prevents incorporating biological channels into membrane selective layers, leading research to focus on synthetic, or artificial channels.

Water channels

Synthetic water channels aim to mimic the separation mechanisms of biological channels that enable their coveted permselectivity. The near-perfect permselectivity of AQP1 is derived from a 3 Å hydrophobic constriction that prevents solute passage based on size and hydrophilicity. Even protons are excluded, due to a charged arginine residue and polar asparagine-proline-alanine motif that disrupt the connectivity of water molecules in the channel [241,242].

Macrocycles–molecules or ions containing one or more rings [243]–have received particular attention as synthetic channel components because of their defined pore sizes and chemically tunable interiors. Macrocycles can be covalently modified or self-assembled to form columnar structures large enough to span an amphiphilic bilayer (Fig. 6a). One example of the latter is π-stacked *m*-phenylene ethynylene macrocycles (6.4 Å pore diameter), which have tailorable interior and exterior surfaces [244]. These *m*-phenylene ethynylene nanotubes allow water permeation but completely reject sodium and lithium ions, demonstrating their remarkable selectivity [244].

Pillar [5]arenes, with pore sizes ~5 Å, are macrocycles with hydroxyl groups that can be appended with peptides to improve water permeability and stability within the supporting matrix [245,246]. Pillar [5]arene channels have reported water permeability within the range of AQP1 (3×10^9 H_2O s^{-1} $channel^{-1}$) but no water/salt selectivity, presumably due to inadequate pore sizes or matrix defects [247]. Peptide-appended hybrid arene channels are similar in nature but have demonstrated dynamic structures, such that water flows through transient pore windows of 5–7 Å dimensions [244]. Up to 10^9 water/salt selectivity was recently reported for peptide-appended hybrid arene channels (Fig. 6b) [244,248], although the mechanisms for salt rejection remain unclear given the pore sizes comparable to those in other studies showing little to no water/salt selectivity [246,247].

Apart from macrocycle-based channels, imidazole-quartet columnar structures (2.6 Å pore diameter) have been self-assembled via π–π interactions and water-assisted hydrogen bonding, and channels were found to transport both water and protons [249]. While the channel completely excludes other ions, water permeability was orders of magnitude lower than AQP1 (Fig. 6b) [237]. It should be noted that with the exception of hybrid arene channels [244], reported water permeabilities were calculated using inaccurate approximations [248]. A more accurate equation was recently presented for approximating water permeability in vesicular systems [250,251].

Ion channels

A distinguishing characteristic between the aquaporin water channel and the K^+ ion channel is that the latter preferentially transports a larger dehydrated species (K^+) over a smaller dehydrated species (Na^+). To accomplish such a separation, a narrow constriction of the K^+ channel, called the selectivity filter, forces ions to remove their solvation shells. Then, oriented helices point partially negative carbonyl groups toward the selectivity

filter to provide stabilizing host–guest interactions that offset the energetic cost of K^+ dehydration and reduce its energy barrier of transport [252–254]. These synergistic effects allow ultra-selective conduction of K^+, whereas carbonyl oxygen atoms cannot closely approach a Na^+ ion with its smaller radius [255]. This selectivity mechanism of the KcsA K^+ channel, among other biological channels, has inspired the development of synthetic ion channels.

Macrocycles, such as crown ethers, have been used for artificial ion channels and have demonstrated unique transport sequences where larger cations preferentially pass through the structure. Macrocycle-based molecules can either be covalently affixed on a central scaffolding or stacked via non-covalent forces to form channels. As examples of the former, a pillararene scaffold can be flanked with crown ether [256] or cyclodextrin [257] arms that control the entrance and exit of the channel. The length of the linker connecting the scaffold and flank controls the distance between binding sites and rigidity of the structure, which may affect selectivity [257].

More promising selectivities, however, have been demonstrated with supramolecular channels formed via non-covalent stacking of macrocycles. Eight crown ether-containing molecules were screened as building blocks for a columnar assembly stabilized by hydrogen bonds [258]. Tuning the side chains appended to the crown ethers optimized the self-assembly process, thereby improving the K^+/Na^+ permeability ratio to surpass naturally occurring gramicidin A (Fig. 6b) [258]. The *m*-phenylene ethynylene nanotubes mentioned earlier were also shown to exhibit remarkable H^+/Cl^- and K^+/Cl^- permeability ratios of ~3000 and ~2000, respectively [244].

Non-covalent interactions may form channels via foldamers, molecules that naturally form helical structures. A recent demonstration produced a foldamer channel with a pore diameter of 0.3 nm and a helical height of up to 2.7 nm. The channel resulted in an impressive K^+/Na^+ permeability ratio of ~16.3, although the selectivity of artificial ion channels remains substantially lower than the KcsA K^+ channel (Fig. 6b) [259]. Further selectivity improvements will require channel synthesis techniques that allow for simultaneous control over channel alignment, aspect ratio, binding site distance, and interior and exterior properties.

Challenges in membrane fabrication

One of the primary obstacles to up-scaling biological and biomimetic membranes is to insert aligned, densely packed channels into defect-free membrane selective layers. While several fabrication methods have been applied, channels are generally inserted and aligned in amphiphilic block copolymer bilayers, which have greater chemical and mechanical stability than naturally occurring phospholipids [254,260]. Many studies use low channel-to-amphiphilic molecule ratios to form unilamellar vesicles via detergent dialysis techniques (Fig. 6c, left and middle) [246,261], but vesicles have not been translated into planar, defect-free selective layers. For some channel types, higher channel-to-amphiphilic molecule ratios (>~0.6) form two-dimensional crystalline nanosheets (Fig. 6c, right), which then can be deposited onto porous support layers [246,247]. These nanosheets have increased channel packing densities, but a layer-by-layer technique is needed to conceal framework defects that may limit the attainable permselectivity, similar to graphene oxide laminate membranes [262]. Other losses in selective performance may arise from the lipid or block copolymer matrices, which are permeable to hydrophobic solutes as described by Overton's rule [263]. A low-permeability support layer would help mitigate the loss of membrane selectivity arising due to defects or the amphiphilic matrix but at the cost of permeability [264]. These challenges highlight the need for bottom-up fabrication methods that eliminate transport through defects and the supporting matrix but provide scalability for industrial application.

Process aspects

Membrane materials provide an intrinsic selectivity and permeability for water or target solutes. When membranes are applied in a water treatment process, the overall selectivity is strongly affected by the conditions used in the process, including driving force (e.g., applied pressure or voltage), hydrodynamic conditions, and receiving phase composition, as well as feed water quality [269].

Driving force. The effect of driving force on membrane selectivity varies in different systems. In RO and NF processes, salt rejection increases asymptotically with applied pressure because water flux increases faster than ion flux. In UF processes, membrane pore size can be expanded at high pressure [270], resulting in decreased solute rejection. For IEMs and LMs, selective permeation causes accumulation of competing ions and depletion of target ions in the boundary layer facing the feed side [16,271]. As a result, increasing driving force such as electric field intensity in ED processes would cause a decrease of permselectivity. In thermally driven systems such as MD and pervaporation, the effect of temperature on selectivity is determined by vapor pressure of water relative to other volatile compounds. For example, as the vapor pressure of water increases much faster than HCl with temperature, high temperature operation favours HCl rejection and improves permselectivity of water [272].

Receiving phase composition. In chemical potential-driven systems such as FO and LMs, the composition of the receiving phase affects the concentration gradient of target species and hence transport driving force. FO draw solutions contain ultrahigh concentrations of inorganic/organic compounds (e.g., NaCl, Na_2SO_4, NH_4HCO_3, and sucrose) [273], while LMs may use strong acid [227,233] or organic solvents as stripping solutions. Receiving solutions that react with the target species (e.g., acid or base solutions to absorb NH_3 and HCl in MD and pervaporation systems) enhance the selectivity of these target species by lowering their concentration on the permeate side.

Other important factors affecting membrane selectivity include operating temperature, flow rate, and feed pH. Increasing temperature accelerates solute diffusivity in RO and NF membranes, thus decreasing solute rejection [274,275]. Higher cross-flow velocity enhances solute mass transfer to the membrane surface, and improves the selectivity for target ions in IEM, FO, and LM systems. Solution pH affects selectivity by altering the charge interaction between the membrane and the solutes. Furthermore, membrane selectivity is subject to the negative

impacts of long-term operational problems, including fouling [22,276,277], MD membrane wetting [278], and membrane material degradation [279,280]. Therefore, membrane materials that are fouling- and scaling-resistant and have higher chemical stability will be better able to maintain their selectivity.

Outlook

A number of novel materials have shown promise as high selectivity membranes for desalination, water purification and resource recovery. In particular, materials that are prepared using the bottom-up approach demonstrate great versatility and tuneability necessary for removing the wide range of chemicals encountered in water and wastewater treatment. Nevertheless, the development of these novel membrane materials is still in its infancy, and needs to transcend a number of challenges before practical application can be achieved. In particular, developing scalable fabrication methods to produce large, high quality, mechanically robust, and chemically stable water treatment membranes using these novel materials remains a critical research need. Furthermore, chemical transport mechanisms in composite IEMs, biological channels, and some MOFs/COFs are not well understood, which hinders further development of these membrane materials. Advanced simulation and characterization methods at the molecular or atomic levels are needed to investigate the specific solute-membrane interactions under the various types of driving forces, as well as the roles of membrane physicochemical properties (e.g., pore size and geometry, charge density, and distribution). Finally, the success of these membrane materials for practical application depends strongly on the availability, cost, safety, and environmental footprint of raw materials as well as that of the cost and scalability of the fabrication processes. Non-toxic, earth-abundant raw materials and environment-friendly synthesis methods should be used whenever possible to avoid health and environmental risks; secure immobilization of functional additives (e.g., engineered nanomaterials, solvents for LMs) is critical to not only product safety but also longevity. Current literature suggests that significant research and development is needed before precise porous membrane materials (e.g., 2D laminar materials, MOFs, and COFs) and dense IEMs and LMs becomes commercially viable; whereas bio-inspired membranes offer the most promise in terms of separation performance [281], they are the farthest from commercial reality.

High selectivity and permeability membrane materials will play a major role in future water systems, where the vision of "one water" [282,283] is realized by integrated water management with distributed, fit-for-purpose water treatment [284,285]. In such integrated water management systems, high-rate, precise separation of chemicals from water is necessary not only for pollution control, but also for minimization of chemical and energy consumption, and for recycling and reuse of resources. For example, highly selective NF membranes prepared with 2D laminar materials or isoporous MOF/COF will remove toxic organics and heavy metals while preserving sufficient essential minerals in drinking water production from both conventional and alternative water sources. Selective IEMs and LMs could be used to recover nitrogen and phosphorous from municipal wastewater as well as other valuable chemicals from industrial wastewaters, to remove mineral scalants, and for other fit-for-purpose treatment of industrial wastewater. These capabilities will enable high energy efficiency, low-cost, and environmentally sustainable treatment processes necessary for future water systems.

Author contributions

K.Z., K.W., R.M.D., Q.F., E.M.D., R.X. and I.A. primarily wrote the manuscript. Q.L., X.H., M.E. and J.L. gave significant input for overall article content and organization as primary advisors for this work. X.H., Z.H., Y.F. and W.S.W. provided technical feedback and helped revise the manuscript.

CRediT authorship contribution statement

Kuichang Zuo: Conceptualization, Writing - original draft, Writing - review & editing. **Kunpeng Wang:** Writing - original draft. **Ryan M. DuChanois:** Writing - original draft, Writing - review & editing. **Qiyi Fang:** Writing - original draft. **Eva M. Deemer:** Writing - original draft. **Xiaochuan Huang:** Writing - original draft, Writing - review & editing. **Ruikun Xin:** Writing - original draft. **Ibrahim A. Said:** Writing - original draft. **Ze He:** Writing - original draft. **Yuren Feng:** Writing - original draft. **W. Shane Walker:** Supervision. **Jun Lou:** Supervision, Writing - review & editing. **Menachem Elimelech:** Supervision, Writing - review & editing. **Xia Huang:** Supervision, Writing - review & editing. **Qilin Li:** Conceptualization, Supervision, Writing - original draft, Writing - review & editing.

Declaration of Competing Interest

The authors declare that they have no known competing financial interests or personal relationships that could have appeared to influence the work reported in this paper.

Acknowledgements

This work was supported by the NSF Nanosystems Engineering Research Center for Nanotechnology-Enabled Water Treatment (EEC-1449500). We also acknowledge the NSF Graduate Research Fellowship and the Abel Wolman Fellowship from the American Water Works Association awarded to R.M.D.

Appendix A. Supplementary data

Supplementary data to this article can be found online at https://doi.org/10.1016/j.mattod.2021.06.013.

References

[1] D.M. Warsinger et al., Prog. Polym. Sci. 81 (2018) 209.
[2] J. Sun et al., Water Res.. 93 (2016) 205.
[3] Y.X. Shen et al., J. Membrane Sci. 415 (2012) 336.
[4] S. Muthukumaran et al., J. Membrane Sci. 258 (1–2) (2005) 106.
[5] J.Q. Luo et al., Bioresour. Technol. 102 (16) (2011) 7437.
[6] F. Lipnizki, Eng. Life Sci. 5 (1) (2005) 81.
[7] S. Jamaly et al., Desalination 354 (2014) 30.
[8] A. Kamble, Membrane Microfiltration Market by Filtration mode, Material, and End user - Global Opportunity Analysis and Industry Forecast, 2014-2022; A01556, Allied Market Research, 2017.
[9] B.P. Staff, Ultrafiltration Membranes: Technologies and Global Markets; MST044E, BCC Research, 2020.
[10] Z.Y. Wang et al., Nat. Commun. (2018) 9.

[11] L.F. Greenlee et al., Water Res.. 43 (9) (2009) 2317.
[12] J.R. McCutcheon et al., Desalination 174 (1) (2005) 1.
[13] S. Kumar, R. Deshmukh, Reverse Osmosis Membrane Market by Material Type, Filter Module and Application: Global Opportunity Analysis and Industry Forecast, 2018-2025; A01305, Allied Market Res., 2019.
[14] Choudhary, A., et al., Nanofiltration Membrane Market by Type and Application: Global Opportunity Analysis and Industry Forecast, 2018 - 2025; A03697, Allied Market Research, 2019.
[15] P.D. Dongare et al., Proc. Natl. Acad. Sci. U. S. A. 114 (27) (2017) 6936.
[16] T. Luo et al., J Membr. Sci 555 (2018) 429.
[17] R.C. Smith et al., Environ. Sci. Technol. 53 (8) (2019) 4490.
[18] D. Kim et al., Environ. Sci. Technol. 49 (16) (2015) 9452.
[19] J.F. Wang et al., Green Energy Environ.. 1 (1) (2016) 43.
[20] World Health O., Guidelines for Drinking-Water Quality: Fourth Edition Incorporating First Addendum, 4th ed + 1st add ed.;., World Health Organization:, Geneva, 2017.
[21] M.A. Barakat, Arab. J. Chem. 4 (4) (2011) 361.
[22] S. Bolisetty et al., Chem. Soc. Rev. 48 (2) (2019) 463.
[23] N. Abdullah et al., J. Ind. Eng. Chem. 76 (2019) 17.
[24] D.T. Sun et al., J. Am. Chem. Soc. 140 (48) (2018) 16697.
[25] A.C. Ni'am et al., Chem. Eng. Process. Process Intensif. (2020) 148.
[26] D.D. Xu et al., Miner. Eng. (2019) 139.
[27] D. Kim et al., Sep. Sci. Technol. 51 (10) (2016) 1716.
[28] Q. Wang et al., Ind. Eng. Chem. Res. 58 (27) (2019) 12280.
[29] A.J. Ward et al., Water Res. 135 (2018) 57.
[30] F. Harnisch, U. Schroder, ChemSusChem 2 (10) (2009) 921.
[31] X.-Y. Nie et al., J. Membrane Sci. 530 (2017) 185.
[32] L.M. Robeson, J. Membrane Sci. 62 (2) (1991) 165.
[33] Z. Yang et al., J. Membrane Sci. (2019) 590.
[34] G.M. Geise et al., J. Membrane Sci. 369 (1–2) (2011) 130.
[35] Z. Yang et al., Environ. Sci. Technol. 52 (16) (2018) 9341.
[36] A. Mehta, A.L. Zydney, J Membr. Sci 249 (1–2) (2005) 245.
[37] G.M. Geise et al., ACS Appl. Mater. Interfaces 5 (20) (2013) 10294.
[38] D.L. Shaffer et al., Desalination 356 (2015) 271.
[39] H.B. Park et al., Science 356 (2017) 6343.
[40] J.R. Werber et al., Nat. Rev. Mater. 1 (2016) 5.
[41] E. Jones et al., Sci. Total Environ. 657 (2019) 1343.
[42] D.L. Shaffer et al., J. Membrane Sci. 415–416 (2012) 1.
[43] A.W. Mohammad et al., Desalination 356 (2015) 226.
[44] Q. Li et al., J. Membrane Sci. 584 (2019) 324.
[45] P. Marchetti et al., Chem. Rev. 114 (21) (2014) 10735.
[46] T. Xu, J. Membrane Sci. 263 (1–2) (2005) 1.
[47] Y. Mizutani, J. Membrane Sci. 54 (3) (1990) 233.
[48] C.T. Matos et al., Water Res. 42 (6) (2008) 1785.
[49] F. Roghmans et al., J. Membrane Sci. 600 (2020) 117854.
[50] W. Shi et al., Sep. Purif. Technol. 210 (2019) 885.
[51] E. Curcio, E. Drioli, Sep. Purif. Rev. 34 (2005) 35.
[52] A. Alkhudhiri et al., Desalination 287 (2012) 2.
[53] K. Wang et al., Appl. Surf. Sci. 450 (2018) 57.
[54] J.M. Winglee et al., Environ. Sci. Technol. 51 (22) (2017) 13113.
[55] Y. Xiang et al., Langmuir 30 (30) (2014) 9098.
[56] W. Li et al., ACS Nano 12 (9) (2018) 9309.
[57] K. Rathinam et al., Water Res. 128 (2018) 217.
[58] X. Li et al., J. Membrane Sci. 494 (2015) 68.
[59] C.X. Yu et al., Chem. Sci. 8 (11) (2017) 7611.
[60] D. Cohen-Tanugi, J.C. Grossman, Nano Lett. 12 (7) (2012) 3602.
[61] R. Das et al., Desalination 336 (2014) 97.
[62] Y. Gong et al., J. Membrane Sci. (2020) 600.
[63] J.-J. Wang et al., J. Mater. Chem. A 5 (31) (2017) 16289.
[64] G. Gong et al., ACS Appl. Mater. Interfaces 11 (7) (2019) 7349.
[65] Y. Hao et al., J. Mater. Chem. A 8 (10) (2020) 5275.
[66] Z. Wang et al., Nat. Commun. 9 (1) (2018) 2004.
[67] J. Zhu et al., J. Mater. Chem. A 6 (32) (2018) 15701.
[68] L. Bai et al., Environ. Sci. Technol. 52 (19) (2018) 11178.
[69] D. Qin et al., J. Membrane Sci. (2020) 603.
[70] Z. Tan et al., Science 360 (6388) (2018) 518.
[71] C. Jiang et al., J. Membrane Sci. 586 (2019) 192.
[72] C. Jiang et al., J. Membrane Sci. 589 (2019) 117244.
[73] W. Shang et al., J. Membrane Sci. (2020) 600.
[74] C.-E. Lin et al., J. Membrane Sci. 518 (2016) 72.
[75] D.M. Kanani et al., J. Membrane Sci. 349 (1–2) (2010) 405.
[76] M. Sun et al., Adv. Funct. Mater. 29 (2019) 36.
[77] M. Shaban et al., Chem. Eng. Res. Des. 95 (2015) 307.
[78] M. Bhadra et al., Desalination 341 (2014) 115.
[79] Z.-Q. Dong et al., Desalination 347 (2014) 175.
[80] T.L.S. Silva et al., Desalination 357 (2015) 233.
[81] L.F. Dumee et al., J. Membrane Sci. 351 (1–2) (2010) 36.
[82] Y.X. Huang et al., J. Membrane Sci. 531 (2017) 122.
[83] S.R. Krajewski et al., J. Membrane Sci. 281 (1–2) (2006) 253.
[84] S. Leaper et al., J. Membrane Sci. 554 (2018) 309.
[85] Y. Liao et al., J. Membrane Sci. 425 (2013) 30.
[86] K.J. Lu et al., J. Membrane Sci. 539 (2017) 34.
[87] L.D. Tijing et al., J. Membrane Sci. 502 (2016) 158.
[88] Y.C. Woo et al., J. Membrane Sci. 520 (2016) 99.
[89] M. Bhadra et al., Sep. Purif. Technol. 120 (2013) 373.
[90] R.R. Nair et al., Science 335 (6067) (2012) 442.
[91] D.A. Dikin et al., Nature 448 (7152) (2007) 457.
[92] R.K. Joshi et al., Science 343 (6172) (2014) 752.
[93] C.E. Ren et al., J. Phys. Chem. Lett. 6 (20) (2015) 4026.
[94] L. Ding et al., Angew. Chem. Int. Ed. 56 (7) (2017) 1825.
[95] L. Ding et al., Nat. Commun. 9 (1) (2018) 155.
[96] H. Huang et al., Nat. Commun. 4 (1) (2013) 2979.
[97] K. Huang et al., Angew. Chem. Int. Ed. 53 (27) (2014) 6929.
[98] Y. Han et al., Adv. Funct. Mater. 23 (29) (2013) 3693.
[99] B. Qian et al., Adv. Mater. Interfaces 2 (16) (2015) 1500372.
[100] C. Chi et al., Chem. Mater. 28 (9) (2016) 2921.
[101] K.-H. Lee et al., Carbon 83 (2015) 40.
[102] L. Chen et al., Nature 550 (7676) (2017) 415.
[103] Z.Q. Jia, Y. Wang, J. Mater. Chem. A 3 (8) (2015) 4405.
[104] S. Kim et al., J. Mater. Chem. A 5 (4) (2017) 1533.
[105] W.X. Zhang et al., J. Mater. Chem. A 6 (27) (2018) 13331.
[106] W.S. Hummers, R.E. Offeman, J. Am. Chem. Soc. 80 (6) (1958) 1339.
[107] D.R. Dreyer et al., Chem. Soc. Rev. 39 (1) (2010) 228.
[108] D.W. Boukhvalov et al., Nano Lett. 13 (8) (2013) 3930.
[109] K. Raidongia, J. Huang, J. Am. Chem. Soc. 134 (40) (2012) 16528.
[110] O.C. Compton, S.T. Nguyen, Small 6 (6) (2010) 711.
[111] C.-N. Yeh et al., Nat. Chem. 7 (2) (2015) 166.
[112] Y. Su et al., Nat. Commun. 5 (1) (2014) 4843.
[113] C.A. Amadei et al., Environ. Sci. Technol. 51 (8) (2017) 4280.
[114] M.J. McAllister et al., Chem. Mater. 19 (18) (2007) 4396.
[115] G. Williams et al., ACS Nano 2 (7) (2008) 1487.
[116] R.S. Sundaram et al., Adv. Mater. 20 (16) (2008) 3050.
[117] H.-H. Huang et al., J. Membrane Sci. 572 (2019) 12.
[118] E. Yang et al., J. Membrane Sci. 547 (2018) 73.
[119] H. Liu et al., Adv. Mater. 27 (2) (2015) 249.
[120] Y.Z. Zhang et al., J. Membrane Sci. 563 (2018) 718.
[121] W.S. Hung et al., Chem. Mater. 26 (9) (2014) 2983.
[122] J. Su et al., Environ. Sci. Nano 7 (10) (2020) 2924.
[123] W.Y. Xing et al., Mater. Des. 115 (2017) 46.
[124] M.Y. Lim et al., J. Membrane Sci. 521 (2017) 1.
[125] S. Rajesh, A.B. Bose, ACS Appl. Mater. Interfaces 11 (31) (2019) 27706.
[126] T. Liu et al., J. Membrane Sci. 542 (2017) 31.
[127] M. Chhowalla et al., Nat. Chem. 5 (4) (2013) 263.
[128] L. Ries et al., Nat. Mater. 18 (10) (2019) 1112.
[129] W. Hirunpinyopas et al., ACS Nano 11 (11) (2017) 11082.
[130] L.W. Sun et al., Chem. Commun. 49 (91) (2013) 10718.
[131] L. Sun et al., ACS Nano 8 (6) (2014) 6304.
[132] H. Li et al., Nano Lett. 19 (8) (2019) 5194.
[133] M. Naguib et al., Adv. Mater. 26 (7) (2014) 992.
[134] Karahan, H. E., et al., Adv. Mater. n/a (n/a), 1906697.
[135] C.E. Ren et al., ACS Appl. Nano Mater. 1 (7) (2018) 3644.
[136] C.E. Ren et al., J. Phys. Chem. Lett. 6 (20) (2015) 4027.
[137] L. Ding et al., Nat. Sustainability 3 (4) (2020) 296.
[138] Z. Lu et al., ACS Nano 13 (9) (2019) 10535.
[139] X. Lu et al., Environ. Sci. Technol. 54 (15) (2020) 9640.
[140] Y. Su et al., ACS Appl. Mater. Interfaces 12 (40) (2020) 45453.
[141] M.M. Chen et al., J. Mater. Chem. A 5 (32) (2017) 17029.
[142] Y.B. Yang et al., Science 364 (6445) (2019) 1057.
[143] S.P. Surwade et al., Nat. Nanotechnol. 10 (5) (2015) 459.
[144] J.W. Shen et al., Desalination 395 (2016) 28.
[145] B. Corry, J. Phys. Chem. B 112 (5) (2008) 1427.
[146] B.J. Hinds et al., Science 303 (5654) (2004) 62.
[147] J.K. Holt et al., Science 312 (5776) (2006) 1034.
[148] Y. Baek et al., Desalin. Water Treat. 57 (58) (2016) 28133.
[149] K.J. Lee, H.D. Park, J. Membrane Sci. 501 (2016) 144.
[150] B. Lee et al., Nat. Commun. (2015) 6.

[151] H.-C. Zhou et al., Chem. Rev. 112 (2) (2012) 673.
[152] N. Huang et al., Nat. Rev. Mater. 1 (10) (2016) 16068.
[153] A.P. Côté et al., Science 310 (5751) (2005) 1166.
[154] C. Zhang et al., Chem. Soc. Rev. 48 (14) (2019) 3811.
[155] X. Li et al., Chem. Soc. Rev. 46 (23) (2017) 7124.
[156] Y. Guo et al., Appl. Mater. Today 5 (2016) 103.
[157] C. Liu et al., ACS Appl. Mater. Interfaces 12 (2) (2020) 2816.
[158] X.L. Liu et al., J. Am. Chem. Soc. 137 (22) (2015) 6999.
[159] X. Li et al., Nat. Commun. 10 (1) (2019) 2490.
[160] R.B. Stockbridge et al., Nature 525 (7570) (2015) 548.
[161] J. Lu et al., Nat. Mater. 19 (7) (2020) 767.
[162] M.S. Lohse, T. Bein, Adv. Funct. Mater. 28 (2018) 33.
[163] H. Wang et al., Chem. Soc. Rev. 48 (2) (2019) 488.
[164] Z.F. Wang et al., Chem. Soc. Rev. 49 (3) (2020) 708.
[165] S.S. Yuan et al., Chem. Soc. Rev. 48 (10) (2019) 2665.
[166] R. Wang et al., J. Membrane Sci. 566 (2018) 197.
[167] R. Wang et al., J. Membrane Sci. 586 (2019) 274.
[168] F.S. Pan et al., Sep. Purif. Technol. 215 (2019) 582.
[169] I. Gadwal et al., ACS Appl. Mater. Interfaces 10 (15) (2018) 12295.
[170] W. Zhou et al., ACS Appl. Mater. Interfaces 11 (18) (2019) 16847.
[171] X.S. Shi et al., J. Membrane Sci. 576 (2019) 116.
[172] M.Y. Wu et al., J. Membrane Sci. 576 (2019) 131.
[173] L. Xu et al., J. Membrane Sci. 526 (2017) 355.
[174] H.W. Fan et al., Angew. Chem. Int. Ed. 57 (15) (2018) 4083.
[175] H. Yang et al., Nat. Commun. (2019) 10.
[176] L.C. Lin et al., Chem. Commun. 51 (80) (2015) 14921.
[177] K. Zhang et al., Environ Sci-Wat Res 3 (4) (2017) 735.
[178] C. Liu et al., J. Mater. Chem. A 7 (42) (2019) 24205.
[179] A.R. Corcos et al., ACS Materials Letters 1 (4) (2019) 440.
[180] X.K. Zhang et al., J. Membrane Sci. 581 (2019) 321.
[181] M. Jian et al., Sci. Adv. 6 (23) (2020) eaay3998.
[182] H. Ang, L. Hong, ACS Appl. Mater. Interfaces 9 (33) (2017) 28079.
[183] J. Dechnik et al., Angew. Chem. Int. Ed. 56 (32) (2017) 9292.
[184] S. Sorribas et al., J. Am. Chem. Soc. 135 (40) (2013) 15201.
[185] L. Chen et al., Appl. Mater. Today 20 (2020) 100791.
[186] D.L. Gin et al., Macromol. Rapid Commun. 29 (5) (2008) 367.
[187] T. Kato et al., Angew. Chem. Int. Ed. 57 (16) (2018) 4355.
[188] D.J. Mulder et al., Chem. Mater. 29 (16) (2017) 6601.
[189] S.J.A. Houben et al., ACS Appl. Mater. Interfaces 13 (6) (2021) 7592.
[190] M.J. Zhou et al., J. Am. Chem. Soc. 129 (31) (2007) 9574.
[191] T. Kato et al., Angew. Chem. Int. Ed. 57 (16) (2018) 4356.
[192] S.T. Ren et al., Front, Environ. Sci. Eng. 11 (2017) 4.
[193] K.C. Zuo et al., Environ. Sci. Technol. 50 (13) (2016) 7254.
[194] J. Pan et al., Energy Environ. Sci. 7 (1) (2014) 354.
[195] K. Zuo et al., Environ. Sci. Technol. 54 (20) (2020) 13322.
[196] K.C. Zuo et al., Environ. Sci. Technol. 52 (16) (2018) 9486.
[197] X. Zhang et al., Environ. Sci. Water Res. Technol. (2020).
[198] J. Ma et al., ACS ES&T Eng. (2020).
[199] K.C. Zuo et al., Desalination 423 (2017) 104.
[200] S.J. Wu et al., Electrochim. Acta 161 (2015) 245.
[201] K.C. Zuo et al., J. Membrane Sci. 547 (2018) 34.
[202] K.C. Zuo et al., Environ. Sci.-Water Res. 2 (5) (2016) 832.
[203] K.-D. Kreuer et al., Chem. Rev. 104 (10) (2004) 4637.
[204] V.I. Zabolotsky, V.V. Nikonenko, J. Membrane Sci. 79 (2) (1993) 181.
[205] G.M. Geise et al., J. Membrane Sci. 423–424 (2012) 195.
[206] G.M. Geise et al., Prog. Polym. Sci. 39 (1) (2014) 1.
[207] F. Helfferich, Ion Exchange. New York, 1962.
[208] T. Luo et al., J. Membrane Sci. 597 (2020) 117645.
[209] K.C. Zuo et al., Bioresour. Technol. 146 (2013) 637.
[210] J. Kim et al., Water Res. 160 (2019) 445.
[211] Y. Zhang et al., J. Membrane Sci. 332 (1) (2009) 104.
[212] J.B. Liao et al., J. Membrane Sci. (2020) 599.
[213] G.S. Gohil et al., J. Membrane Sci. 280 (1) (2006) 210.
[214] X.-Y. Nie et al., Desalination 403 (2017) 128.
[215] N. White et al., ACS Appl. Mater. Interfaces 7 (12) (2015) 6620.
[216] N. Ul Afsar et al., Desalination 458 (2019) 25.
[217] T. Sata, J. Membrane Sci. 167 (1) (2000) 1.
[218] Y.F. Zhang et al., Sep. Purif. Technol. 192 (2018) 278.
[219] T.R. Farhat, J.B. Schlenoff, Langmuir 17 (4) (2001) 1184.
[220] C. Cheng et al., Langmuir 29 (6) (2013) 1885.
[221] N. White et al., Polymer 103 (2016) 478.
[222] Y. Zhao et al., J. Membrane Sci. 520 (2016) 262.
[223] Y. Zhao et al., J. Membrane Sci. 548 (2018) 81.
[224] P.D. Ola, M. Matsumoto, Supported Ionic Liquid Membranes for Metal Separation (2017) 539.
[225] N.N. Li, AIChE J. 17 (2) (1971) 459.
[226] P.K. Parhi, J. Chem. (2013).
[227] V.G. Deshmane et al., Environ. Sci. Technol. 54 (1) (2020) 550.
[228] W. Du et al., Food Chem. 259 (2018) 73.
[229] Y.W. Choi, S.H. Moon, Sep. Sci. Technol. 39 (7) (2005) 1663.
[230] R.A. Kumbasar, J. Membrane Sci. 325 (1) (2008) 460.
[231] Y. Y ld z et al., Desalin. Water Treat. 57 (10) (2016) 4616.
[232] Z.Y. Wang et al., Sep. Purif. Technol. 222 (2019) 136.
[233] Z.W. Zhao et al., J. Membrane Sci. (2020) 596.
[234] M.W. Ashraf et al., Int. J. Environ. Res. Public Health 16 (2019) 18.
[235] A. Fortuny et al., Desalination 343 (2014) 54.
[236] C.J. Porter et al., ACS Nano 14 (9) (2020) 10894.
[237] P. Agre, Angew. Chem. Int. Ed. 43 (33) (2004) 4278.
[238] J.S. Hub, B.L. de Groot, Proc. Natl. Acad. Sci. U.S.A. (2008) 105 (4), 1198.
[239] W. Kopec et al., Nat. Chem. 10 (8) (2018) 813.
[240] D.A. Doyle et al., Science 280 (5360) (1998) 69.
[241] K. Murata et al., Nature 407 (6804) (2000) 599.
[242] U. Kosinska Eriksson et al., Science 340 (6138) (2013) 1346.
[243] S. Vendeville, M.D. Cummings, Chapter Twenty-three - synthetic macrocycles in small-molecule drug discovery, in: Annu. Rep. Med. Chem., M.C. Desai, (ed.) Academic Press (2013), Vol. 48, pp 371.
[244] X. Zhou et al., Nat. Commun. 3 (1) (2012) 949.
[245] L. Chen et al., J. Am. Chem. Soc. 135 (6) (2013) 2152.
[246] Y.-X. Shen et al., Proc. Natl. Acad. Sci. 112 (32) (2015) 9810.
[247] Y.-X. Shen et al., Nat. Commun. 9 (1) (2018) 2294.
[248] W. Song et al., Nat. Nanotechnol. 15 (1) (2020) 73.
[249] Y. Le Duc et al., Angew. Chem. Int. Ed. 50 (48) (2011) 11366.
[250] A. Horner et al., Sci. Adv. 1 (2) (2015) e1400083.
[251] C. Hannesschläger et al., Sci. Rep. 8 (1) (2018) 8516.
[252] Y. Zhou et al., Nature 414 (6859) (2001) 43.
[253] A.N. Thompson et al., Nat. Struct. Mol. Biol. 16 (12) (2009) 1317.
[254] R. Epsztein et al., Nat. Nanotechnol. 15 (6) (2020) 426.
[255] Y. Zhou, R. MacKinnon, J. Mol. Biol. 333 (5) (2003) 965.
[256] W.-X. Feng et al., Org. Lett. 19 (6) (2017) 1438.
[257] P. Xin et al., Angew. Chem. Int. Ed. 58 (9) (2019) 2779.
[258] C. Ren et al., J. Am. Chem. Soc. 139 (36) (2017) 12338.
[259] F. Chen et al., Angew. Chem. Int. Ed. 59 (4) (2020) 1440.
[260] J. Kowal et al., ACS Macro Lett. 3 (1) (2014) 59.
[261] Y. Zhao et al., J. Membrane Sci. 423–424 (2012) 422.
[262] C.L. Ritt et al., Environ. Sci. Technol. 53 (11) (2019) 6214.
[263] J.R. Werber, M. Elimelech, Sci. Adv. 4 (6) (2018) eaar8266.
[264] J.R. Werber et al., Environ. Sci. Technol. 52 (18) (2018) 10737.
[265] R.H. Tunuguntla et al., Science 357 (6353) (2017) 792.
[266] M.J. Borgnia et al., J. Mol. Biol. 291 (5) (1999) 1169.
[267] E. Licsandru et al., J. Am. Chem. Soc. 138 (16) (2016) 5403.
[268] M. LeMasurier et al., J. Gen. Physiol. 118 (3) (2001) 303.
[269] W.J. Lau et al., Desalination 287 (2012) 190.
[270] E. Arkhangelsky, V. Gitis, Sep. Purif. Technol. 62 (3) (2008) 619.
[271] Y. Kim et al., Water Res. 46 (7) (2012) 2042.
[272] S. Kalla et al., J. Chem. Technol. Biotechnol. 94 (1) (2019) 63.
[273] Q. Ge et al., J. Membrane Sci. 442 (2013) 225.
[274] M. Mänttäri et al., Desalination 145 (1) (2002) 81.
[275] X. Jin et al., Desalination 239 (1) (2009) 346.
[276] S. Hube et al., Sci. Total Environ. (2020) 710.
[277] R.R. Choudhury et al., J. Mater. Chem. A 6 (2) (2018) 313.
[278] F. Tibi et al., Process Saf. Environ. Prot. 141 (2020) 190.
[279] M. Rezakazemi et al., Environ. Chem. Lett. 16 (2) (2018) 367.
[280] E.M. Deemer et al., Ind. Eng. Chem. Res. 58 (27) (2019) 11964.
[281] M.M. Pendergast, E.M.V. Hoek, Energy Environ. Sci. 4 (6) (2011) 1946.
[282] G.T. Daigger et al., J. Environ. Eng. 145 (2019) 10.
[283] U. Lall, Water Resour. Res. 50 (6) (2014) 5335.
[284] K.R. Zodrow et al., Environ. Sci. Technol. 51 (18) (2017) 10274.
[285] L. Liu et al., Nat. Sustainability 3 (7) (2020) 548.